Supplementary Note: Chiral Floquet Engineering on Topological Fermions in Chiral Crystals

Benshu Fan,[1,2] Wenhui Duan,[1,3,4,*] Angel Rubio,[2,5,6,†] and Peizhe Tang[7,2,‡]

[1] *State Key Laboratory of Low-Dimensional Quantum Physics and Department of Physics, Tsinghua University, Beijing 100084, People's Republic of China*
[2] *Max Planck Institute for the Structure and Dynamics of Matter, Center for Free Electron Laser Science, 22761 Hamburg, Germany*
[3] *Institute for Advanced Study, Tsinghua University, Beijing 100084, People's Republic of China*
[4] *Frontier Science Center for Quantum Information, Beijing 100084, People's Republic of China*
[5] *Nano-Bio Spectroscopy Group, Departamento de Fisica de Materiales, Universidad del País Vasco UPV/EHU- 20018 San Sebastián, Spain*
[6] *Center for Computational Quantum Physics (CCQ), The Flatiron Institute, 162 Fifth avenue, New York NY 10010, USA*
[7] *School of Materials Science and Engineering, Beihang University, Beijing 100191, People's Republic of China*

CONTENTS

* duanw@tsinghua.edu.cn
† angel.rubio@mpsd.mpg.de
‡ peizhet@buaa.edu.cn

Supplementary Note 1. FIRST-PRINCIPLES CALCULATION FOR THE COSI FAMILY IN EQUILIBRIUM

A. Lattice and band structures

The LH and RH chiral semimetal CoSi compounds are related by a mirror symmetry as shown in Supplementary Figure 1(a). We show the three-dimensional BZ of LH and RH CoSi compounds in Supplementary Figure 1(b). The band structures for LH and RH chiral semimetal CoSi are the same, as illustrated in Supplementary Figure 1(c) and Supplementary Figure 1(d) for cases without SOC and Supplementary Figure 1(e) and Supplementary Figure 1(f) for cases with SOC.

The AlPt compound has the same lattice structure and BZ as the CoSi compound. Because of the same band structures of the LH and RH chiral semimetals, here we only show the band structures of LH AlPt compound, as illustrated in Supplementary Figure 2(a) for the case without SOC and in Supplementary Figure 2(b) for the case with SOC.

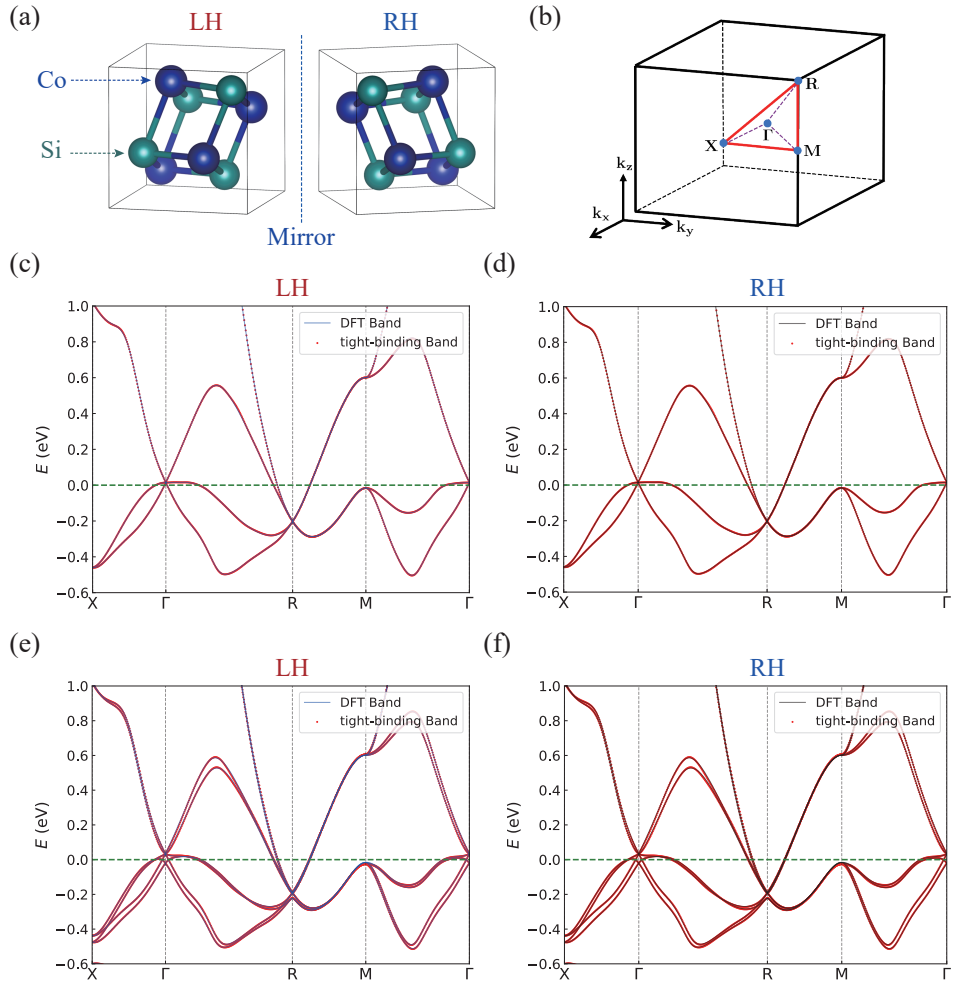

Supplementary Figure 1. (a) The lattice structures for the LH and RH CoSi with opposite chirality are linked by a mirror operation. (b) The BZ of the CoSi family. (c) Comparison of the calculated band structures from DFT calculations in blue lines and tight-binding calculations in red dot lines along high symmetry paths $X \to \Gamma \to R \to M \to \Gamma$ for the LH CoSi without SOC. (d) Similar results as (c) but for the RH CoSi without SOC. (e,f) Corresponding results to (c) and (d) but including the effects of SOC. The Fermi level denoted as the green chain line is set as zero.

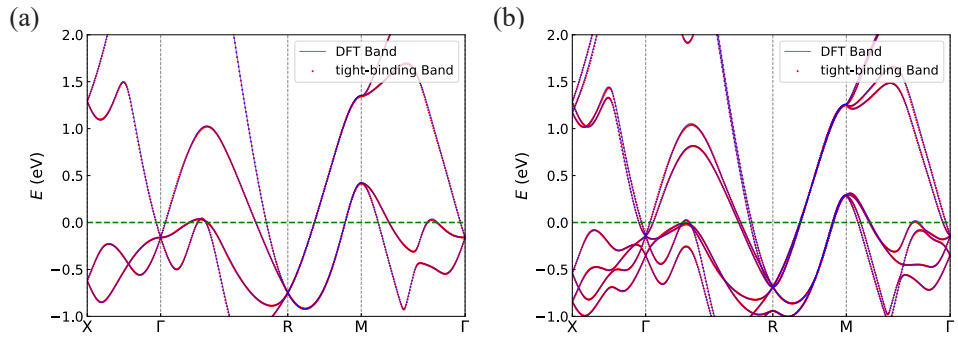

Supplementary Figure 2. (a) Comparison of the calculated band structures from DFT calculations in blue lines and tight-binding calculations in red dot lines along high symmetry paths X $\rightarrow$ Γ $\rightarrow$ R $\rightarrow$ M $\rightarrow$ Γ for the LH AlPt without SOC. (b) Similar results as (a) but for the LH AlPt with SOC. The Fermi level denoted as the green chain line is set as zero.

B. Surface states

As illustrated in Supplementary Figure 3(b) and Supplementary Figure 3(c) for LH and RH CoSi compounds, the Fermi arc states on the (001) surface in Supplementary Figure 3(a) are also related by a mirror operation. As we can see, when we consider the effects of SOC as shown in Supplementary Figure 3(c), the degeneracy of surface states is released. Similar to the case of CoSi compound, we also calculate the (001) surface states of the LH AlPt compound, as shown in Supplementary Figure 4.

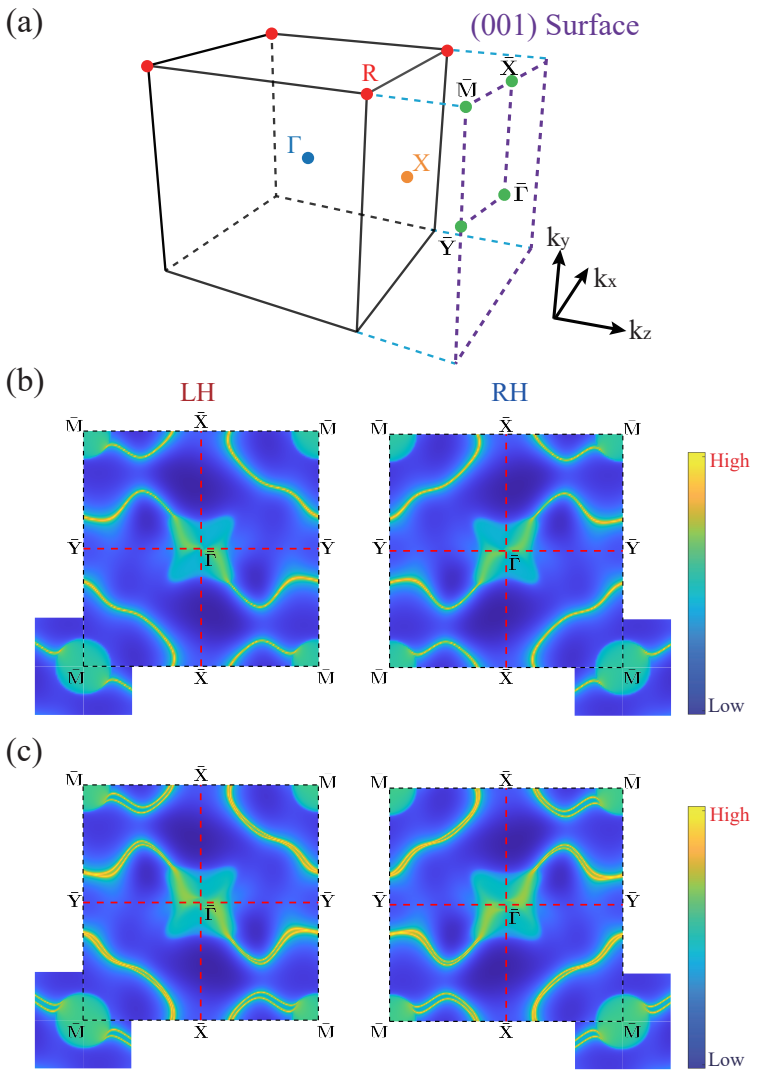

Supplementary Figure 3. (a) The schematic for the BZ of the CoSi compound. The BZ projected on the (001) side surface is marked by purple dashed lines. (b) The Fermi arc states on the (001) surface for the LH (left panel) and RH (right panel) CoSi in equilibrium at the zero-energy cut without SOC. (c) Corresponding results to (b) but including the effects of SOC.

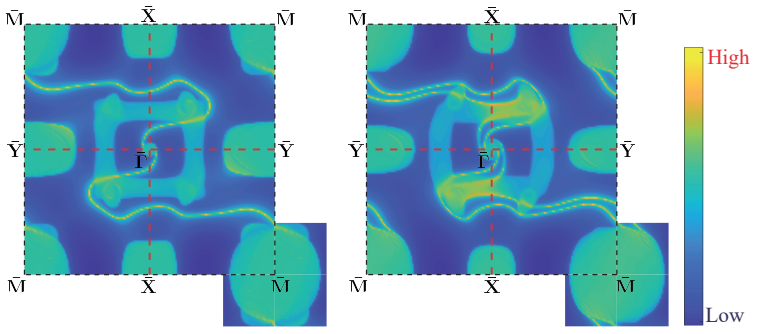

Supplementary Figure 4. The Fermi arc states on the (001) surface for the LH AlPt without SOC (left panel) and with SOC (right panel) in equilibrium at the zero-energy cut.

Supplementary Note 2. FLOQUET EFFECTIVE k · p HAMILTONIAN FOR THE COSI FAMILY

Herein we take the CoSi compound as an example to construct the Floquet effective $\mathbf{k}\cdot\mathbf{p}$ Hamiltonians for the topological fermions at Γ and R points without and with SOC. The Floquet engineering of the linearly polarized light (LPL) has no momentum shift effects on topological fermions at Γ and R points. So we only take the spin-1 excitation as an example to consider the Floquet engineering of the LPL, then consider the pumping of the circularly polarized light (CPL), which is mainly discussed in the main text.

A. Γ point without SOC

The effective $\mathbf{k}\cdot\mathbf{p}$ Hamiltonian of spin-1 excitation at the Γ point [1] is expressed as

$$\hat{H}_\Gamma(\mathbf{k}) = \hbar v_\Gamma \eta \mathbf{k}\cdot\mathbf{J} = \hbar v_\Gamma \eta \begin{pmatrix} 0 & ik_z & -ik_y \\ -ik_z & 0 & ik_x \\ ik_y & -ik_x & 0 \end{pmatrix} \tag{1}$$

where $\mathbf{k} = (k_x, k_y, k_z)$ is the momentum relative to the Γ point, $\hbar v_\Gamma = 1.231$ eV·Å and $\eta = +1(-1)$ for the LH (RH) CoSi [2].

LPL — Here we consider a LPL with the frequency $\Omega = \frac{2\pi}{T}$, where T is one optical cycle, and its polarization aligns with the x direction. The LPL can be represented as $\mathbf{A}(t) = A_0(\sin\Omega t, 0, 0)$, where A_0 denotes the amplitude of the vector potential $\mathbf{A}(t)$. By applying the Peierls substitution $k_x \to k_x + \frac{eA_0}{\hbar}\sin\Omega t$, we obtain the time-dependent $\mathbf{k}\cdot\mathbf{p}$ Hamiltonian for LPL as

$$\hat{H}_\Gamma(\mathbf{k}, t) = \hbar v_\Gamma \eta \begin{pmatrix} 0 & ik_z & -ik_y \\ -ik_z & 0 & ik_x + iA\sin\Omega t \\ ik_y & -ik_x - iA\sin\Omega t & 0 \end{pmatrix} \tag{2}$$

where we have redefined $A = \frac{eA_0}{\hbar}$ for simplicity. Once we assume the photon energy $\hbar\Omega$ is large compared to the other energy scales [3], the perturbation theory can be applied and we obtain the time-independent Floquet effective $\mathbf{k}\cdot\mathbf{p}$ Hamiltonian as

$$\begin{aligned} \hat{H}_\Gamma^{eff}(\mathbf{k}) &= \frac{1}{T}\int_0^T \hat{H}_\Gamma(\mathbf{k}, t)dt + \frac{1}{\hbar\Omega}\sum_{n=1}^{\infty}\frac{1}{n}\left[\hat{H}_n(\mathbf{k}), \hat{H}_{-n}(\mathbf{k})\right] + \mathcal{O}(\Omega^{-2}) \\ &\simeq \frac{1}{T}\int_0^T \hat{H}_\Gamma(\mathbf{k}, t)dt + \frac{1}{\hbar\Omega}\left[\frac{1}{T}\int_0^T e^{-i\Omega t}\hat{H}_\Gamma(\mathbf{k}, t)dt, \frac{1}{T}\int_0^T e^{i\Omega t}\hat{H}_\Gamma(\mathbf{k}, t)dt\right] \end{aligned} \tag{3}$$

where

$$\frac{1}{T}\int_0^T \hat{H}_\Gamma(\mathbf{k}, t)dt = \hbar v_\Gamma \eta \begin{pmatrix} 0 & ik_z & -ik_y \\ -ik_z & 0 & ik_x \\ ik_y & -ik_x & 0 \end{pmatrix} = \hat{H}_\Gamma(\mathbf{k}) \tag{4}$$

$$\frac{1}{T}\int_0^T e^{\mp i\Omega t}\hat{H}_\Gamma(\mathbf{k}, t)dt = \hbar v_\Gamma \eta \begin{pmatrix} 0 & 0 & 0 \\ 0 & 0 & \pm\frac{A}{2} \\ 0 & \mp\frac{A}{2} & 0 \end{pmatrix} \tag{5}$$

and the following formula has been used:

$$\begin{aligned}\frac{1}{T}\int_0^T dt\ \sin\Omega t\, e^{i(n-m)\Omega t} &= \frac{1}{2iT}\int_0^T dt\ \left(e^{i(n-m+1)\Omega t} - e^{i(n-m-1)\Omega t}\right)\\ &= \frac{1}{2i}\left(\delta_{m,n+1} - \delta_{m,n-1}\right)\end{aligned} \tag{6}$$

The second term $M = \frac{1}{\hbar\Omega}\sum_{n=1}^{\infty}\frac{1}{n}\left[\hat{H}_n(\mathbf{k}), \hat{H}_{-n}(\mathbf{k})\right]$ in Supplementary Equation 3 is defined as the Floquet commutator, reflecting the correction of electronic structures due to the light-matter interaction within the perturbation theory. After some calculations, we find the Floquet commutator M in Supplementary Equation 3 is zero and obtain $\hat{H}_\Gamma^{eff}(\mathbf{k}) = \hat{H}_\Gamma(\mathbf{k})$, which has no obvious corrections to the spin-1 excitation. To verify our analysis, we conduct the Floquet tight-binding calculation for this case, as shown in Supplementary Figure 7(a) in Supplementary Note 4 A, and find no obvious momentum shift upon LPL pumping. So next we consider the Floquet engineering of the CPL.

CPL — Let's consider a CPL represented as $\mathbf{A}(t) = A_0(0, \gamma\sin\Omega t, \cos\Omega t)$ incident along the x direction, where $\gamma = \pm 1$ denotes LCPL and RCPL. By applying the Peierls substitution $k_y \to k_y + \gamma\frac{eA_0}{\hbar}\sin\Omega t$ and $k_z \to k_z + \frac{eA_0}{\hbar}\cos\Omega t$, the time-dependent $\mathbf{k}\cdot\mathbf{p}$ Hamiltonian for CPL is obtained as

$$\hat{H}_\Gamma(\mathbf{k}, t) = \hbar v_\Gamma \eta \begin{pmatrix} 0 & ik_z + iA\cos\Omega t & -ik_y - i\gamma A\sin\Omega t \\ -ik_z - iA\cos\Omega t & 0 & ik_x \\ ik_y + i\gamma A\sin\Omega t & -ik_x & 0 \end{pmatrix} \tag{7}$$

where we have redefined $A = \frac{eA_0}{\hbar}$ for simplicity. Using the same method as above, we obtain the time-independent Floquet effective $\mathbf{k}\cdot\mathbf{p}$ Hamiltonian as

$$\hat{H}_\Gamma^{eff}(\mathbf{k}) \simeq \frac{1}{T}\int_0^T \hat{H}_\Gamma(\mathbf{k}, t)dt + \frac{1}{\hbar\Omega}\left[\frac{1}{T}\int_0^T e^{-i\Omega t}\hat{H}_\Gamma(\mathbf{k}, t)dt, \frac{1}{T}\int_0^T e^{i\Omega t}H_\Gamma(\mathbf{k}, t)dt\right] \tag{8}$$

where

$$\frac{1}{T}\int_0^T \hat{H}_\Gamma(\mathbf{k}, t)dt = \hat{H}_\Gamma(\mathbf{k}) \tag{9}$$

$$\frac{1}{T}\int_0^T e^{\mp i\Omega t}\hat{H}_\Gamma(\mathbf{k}, t)dt = \hbar v_\Gamma \eta \begin{pmatrix} 0 & \frac{iA}{2} & \mp\frac{\gamma A}{2} \\ -\frac{iA}{2} & 0 & 0 \\ \pm\frac{\gamma A}{2} & 0 & 0 \end{pmatrix} \tag{10}$$

and the following formula has been used:

$$\begin{aligned}\frac{1}{T}\int_0^T dt\ \cos\Omega t\, e^{i(n-m)\Omega t} &= \frac{1}{2T}\int_0^T dt\ \left(e^{i(n-m+1)\Omega t} + e^{i(n-m-1)\Omega t}\right)\\ &= \frac{1}{2}\left(\delta_{m,n+1} + \delta_{m,n-1}\right)\end{aligned} \tag{11}$$

So finally we obtain

$$\hat{H}_\Gamma^{eff}(\mathbf{k}) = \hbar v_\Gamma \eta \begin{pmatrix} 0 & ik_z & -ik_y \\ -ik_z & 0 & i(k_x - \frac{\gamma v_\Gamma \eta A^2}{2\Omega}) \\ ik_y & -i(k_x - \frac{\gamma v_\Gamma \eta A^2}{2\Omega}) & 0 \end{pmatrix} = \hbar v_\Gamma \eta \left(\mathbf{k}\cdot\mathbf{J} - \frac{\gamma v_\Gamma \eta A^2}{2\Omega}J_x\right) \tag{12}$$

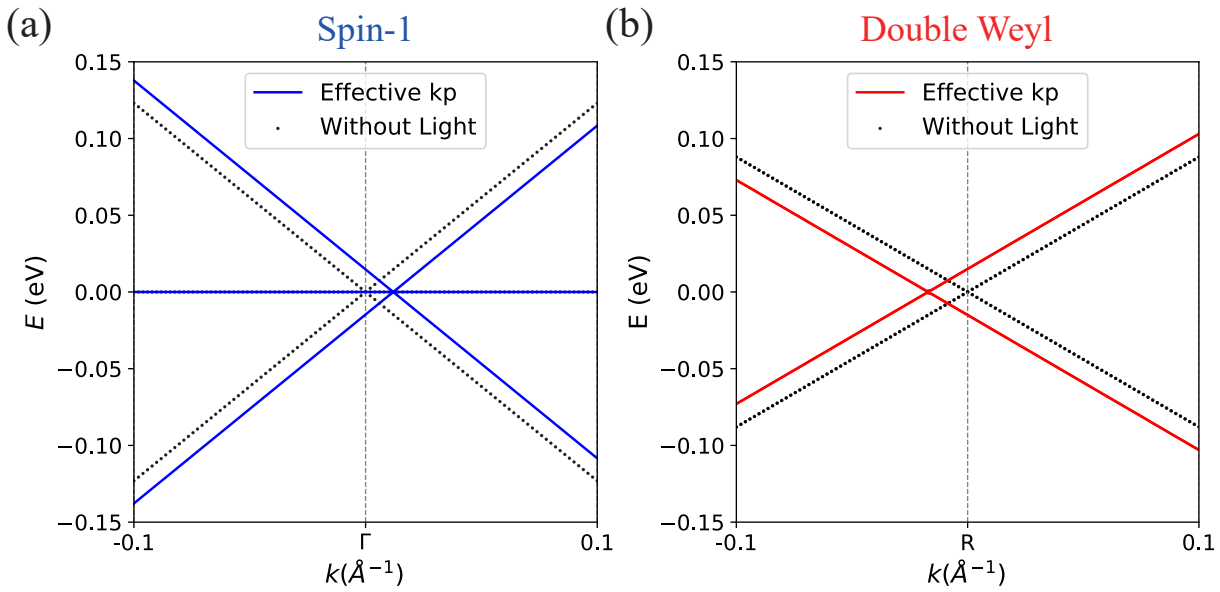

Supplementary Figure 5. (a) Band structures without light pumping in black dot lines and Floquet band structures in blue lines are shown for the spin-1 excitation. (b) Band structures without light pumping in black dot lines and Floquet band structures in red lines are shown for the double Weyl fermion.

As we can see, along the x direction, there is a momentum shift

$$\delta_\Gamma = +\frac{\gamma v_\Gamma \eta A^2}{2\Omega} = \Xi_\Gamma \frac{v_\Gamma}{2} \tag{13}$$

where Ξ_Γ is the Floquet chirality index in the main text. Then we take the LH CoSi ($\eta = +1$) under the pumping of LCPL ($\gamma = +1$) as an example to plot the Floquet band structures, and the results are shown in Supplementary Figure 5(a) in blue lines.

B. R point without SOC

The effective $\mathbf{k}\cdot\mathbf{p}$ Hamiltonian of the double Weyl fermion at the R point [1] is expressed as

$$\hat{H}_{\mathrm{R}}(\mathbf{k}) = \hbar v_{\mathrm{R}} \eta \mathbf{k}\cdot(\boldsymbol{\sigma}\oplus\boldsymbol{\sigma}) = \hbar v_{\mathrm{R}}\eta \begin{pmatrix} \mathbf{k}\cdot\boldsymbol{\sigma} & 0 \\ 0 & \mathbf{k}\cdot\boldsymbol{\sigma} \end{pmatrix} \tag{14}$$

where $\hbar v_{\mathrm{R}} = 0.88$ eV·Å. Actually there are no corrections to the effective $\mathbf{k}\cdot\mathbf{p}$ Hamiltonian for the Floquet engineering of the LPL, leading to the absence of momentum shift, as shown in Supplementary Figure 7(b) in Supplementary Note 4 A. Now we only show the results for the Floquet engineering of the CPL. For a CPL $\mathbf{A}(t) = A_0(0, \gamma\sin\Omega t, \cos\Omega t)$ incident along the x direction, considering the Peierls substitution ($k_y \to k_y + \gamma\frac{eA_0}{\hbar}\sin\Omega t, k_z \to k_z + \frac{eA_0}{\hbar}\cos\Omega t$), we obtain

$$\begin{aligned}&\hat{H}_{\mathrm{R}}(\mathbf{k},t)\\ =&\hbar v_{\mathrm{R}}\eta \begin{pmatrix} k_z + A\cos\Omega t & k_x - ik_y - i\gamma A\sin\Omega t & 0 & 0 \\ k_x + ik_y + i\gamma A\sin\Omega t & -k_z - A\cos\Omega t & 0 & 0 \\ 0 & 0 & k_z + A\cos\Omega t & k_x - ik_y - i\gamma A\sin\Omega t \\ 0 & 0 & k_x + ik_y + i\gamma A\sin\Omega t & -k_z - A\cos\Omega t \end{pmatrix}\end{aligned} \tag{15}$$

where we have redefined $A = \frac{eA_0}{\hbar}$ for simplicity. Using the same method as above, we obtain the time-independent Floquet effective $\mathbf{k}\cdot\mathbf{p}$ Hamiltonian as

$$\hat{H}_{\mathrm{R}}^{eff}(\mathbf{k}) \simeq \frac{1}{T}\int_0^T \hat{H}_{\mathrm{R}}(\mathbf{k},t)dt + \frac{1}{\hbar\Omega}\left[\frac{1}{T}\int_0^T e^{-i\Omega t}\hat{H}_{\mathrm{R}}(\mathbf{k},t)dt, \frac{1}{T}\int_0^T e^{i\Omega t}H_{\mathrm{R}}(\mathbf{k},t)dt\right] \tag{16}$$

where

$$\frac{1}{T}\int_0^T \hat{H}_{\mathrm{R}}(\mathbf{k},t)dt = \hat{H}_{\mathrm{R}}(\mathbf{k}) \tag{17}$$

and

$$\frac{1}{T}\int_0^T e^{\mp i\Omega t}\hat{H}_{\mathrm{R}}(\mathbf{k},t)dt = \hbar v_{\mathrm{R}}\eta\begin{pmatrix} \frac{A}{2} & \mp\frac{\gamma A}{2} & 0 & 0 \\ \pm\frac{\gamma A}{2} & -\frac{A}{2} & 0 & 0 \\ 0 & 0 & \frac{A}{2} & \mp\frac{\gamma A}{2} \\ 0 & 0 & \pm\frac{\gamma A}{2} & -\frac{A}{2} \end{pmatrix} \tag{18}$$

Similarly, we can obtain

$$\hat{H}_{\mathrm{R}}^{eff}(\mathbf{k}) = \hbar v_{\mathrm{R}}\eta\begin{pmatrix} \mathbf{k}\cdot\boldsymbol{\sigma} + \frac{\gamma v_{\mathrm{R}}\eta A^2}{\Omega}\sigma_x & 0 \\ 0 & \mathbf{k}\cdot\boldsymbol{\sigma} + \frac{\gamma v_{\mathrm{R}}\eta A^2}{\Omega}\sigma_x \end{pmatrix} = \hbar v_{\mathrm{R}}\eta\left(\mathbf{k}\cdot(\boldsymbol{\sigma}\oplus\boldsymbol{\sigma}) + \frac{\gamma v_{\mathrm{R}}\eta A^2}{\Omega}\sigma_x\oplus\sigma_x\right) \tag{19}$$

And there is a momentum shift $\delta_{\mathrm{R}} = -\frac{\gamma v_{\mathrm{R}}\eta A^2}{\Omega} = \Xi_{\mathrm{R}} v_{\mathrm{R}}$ along the x direction. Then we take the LH CoSi ($\eta = +1$) under the pumping of LCPL ($\gamma = +1$) as an example to plot the Floquet band structures, the results are shown in Supplementary Figure 5(b) in red lines and the momentum shift is opposite compared to that of the spin-1 excitation in Supplementary Figure 5(a).

C. Γ point with SOC

The effective $\mathbf{k}\cdot\mathbf{p}$ Hamiltonian of the spin-3/2 excitation at the Γ point [4] can be written as

$$\hat{H}_{\Gamma}(\mathbf{k}) = \hbar v_{\Gamma}\eta\mathbf{k}\cdot\mathbf{S}_{\frac{3}{2}} = \hbar v_{\Gamma}\eta\begin{pmatrix} ak_z & 0 & -\frac{a+3b}{4}k_+ & \frac{\sqrt{3}(a-b)}{4}k_- \\ 0 & bk_z & \frac{\sqrt{3}(a-b)}{4}k_- & 0 \\ -\frac{a+3b}{4}k_- & \frac{\sqrt{3}(a-b)}{4}k_+ & -ak_z & 0 \\ \frac{\sqrt{3}(a-b)}{4}k_+ & 0 & 0 & -bk_z \end{pmatrix} \tag{20}$$

where $k_\pm = k_x \pm ik_y$, $a = \cos\epsilon$, $b = \sin\epsilon$, $\epsilon = \arctan(-3)$ and $\hbar v_\Gamma = 1$ eV·Å for simplicity. For a CPL $\mathbf{A}(t) = A_0(0, \gamma\sin\Omega t, \cos\Omega t)$ incident along the x direction, considering the Peierls substitution ($k_y \to k_y + \gamma\frac{eA_0}{\hbar}\sin\Omega t, k_z \to k_z + \frac{eA_0}{\hbar}\cos\Omega t$), we obtain the $\hat{H}_\Gamma(\mathbf{k},t)$ as

$$\hbar v_{\Gamma}\eta\begin{pmatrix} a(k_z + A\cos\Omega t) & 0 & -\frac{a+3b}{4}(k_+ + i\gamma A\sin\Omega t) & \frac{\sqrt{3}(a-b)}{4}(k_- - i\gamma A\sin\Omega t) \\ 0 & b(k_z + A\cos\Omega t) & \frac{\sqrt{3}(a-b)}{4}(k_- - i\gamma A\sin\Omega t) & 0 \\ -\frac{a+3b}{4}(k_- - i\gamma A\sin\Omega t) & \frac{\sqrt{3}(a-b)}{4}(k_+ + i\gamma A\sin\Omega t) & -a(k_z + A\cos\Omega t) & 0 \\ \frac{\sqrt{3}(a-b)}{4}(k_+ + i\gamma A\sin\Omega t) & 0 & 0 & -b(k_z + A\cos\Omega t) \end{pmatrix} \tag{21}$$

where we have redefined $A = \frac{eA_0}{\hbar}$ for simplicity. In the same way, we can calculate that

$$\frac{1}{T}\int_0^T \hat{H}_{\Gamma}(\mathbf{k},t)dt = \hat{H}_{\Gamma}(\mathbf{k}) \tag{22}$$

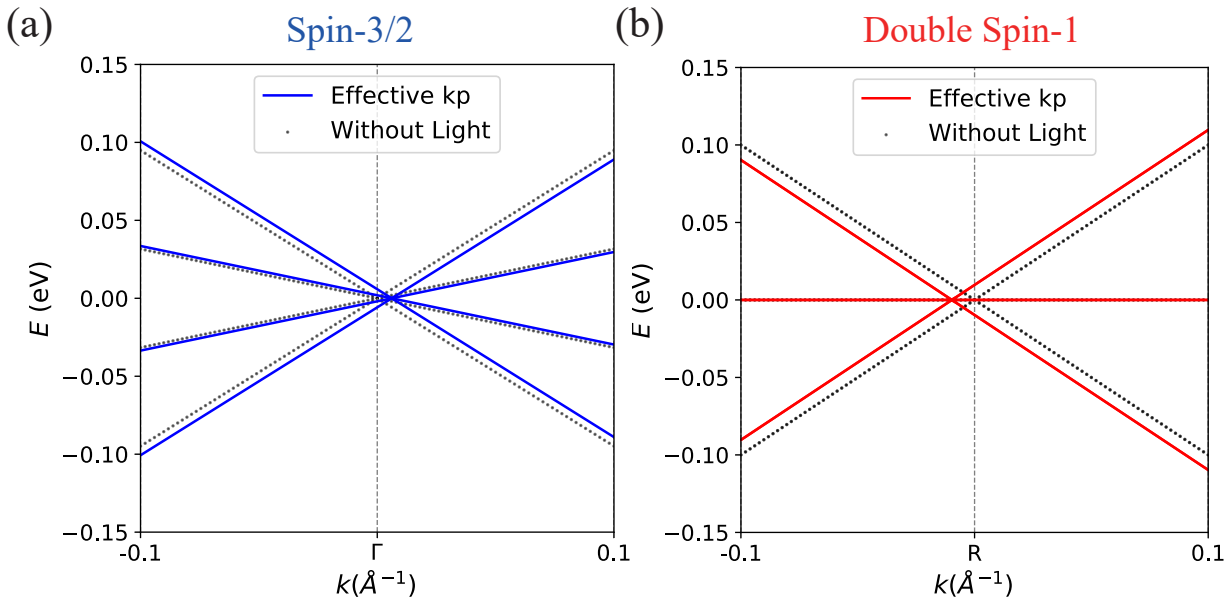

Supplementary Figure 6. (a) Band structures without light pumping in black dot lines and Floquet band structures in blue lines are shown for the spin-3/2 excitation. (b) Band structures without light pumping in black dot lines and Floquet band structures in red lines are shown for the double spin-1 fermion.

and

$$\frac{1}{T}\int_0^T e^{-i\Omega t}\hat{H}_\Gamma(\mathbf{k},t)dt = \hbar v_\Gamma \eta \begin{pmatrix} \frac{aA}{2} & 0 & -\frac{a+3b}{4}\frac{\gamma A}{2} & -\frac{\sqrt{3}(a-b)}{4}\frac{\gamma A}{2} \\ 0 & \frac{bA}{2} & -\frac{\sqrt{3}(a-b)}{4}\frac{\gamma A}{2} & 0 \\ \frac{a+3b}{4}\frac{\gamma A}{2} & \frac{\sqrt{3}(a-b)}{4}\frac{\gamma A}{2} & -\frac{aA}{2} & 0 \\ \frac{\sqrt{3}(a-b)}{4}\frac{\gamma A}{2} & 0 & 0 & -\frac{bA}{2} \end{pmatrix} \tag{23}$$

$$\frac{1}{T}\int_0^T e^{i\Omega t}\hat{H}_\Gamma(\mathbf{k},t)dt = \hbar v_\Gamma \eta \begin{pmatrix} \frac{aA}{2} & 0 & \frac{a+3b}{4}\frac{\gamma A}{2} & \frac{\sqrt{3}(a-b)}{4}\frac{\gamma A}{2} \\ 0 & \frac{bA}{2} & \frac{\sqrt{3}(a-b)}{4}\frac{\gamma A}{2} & 0 \\ -\frac{a+3b}{4}\frac{\gamma A}{2} & -\frac{\sqrt{3}(a-b)}{4}\frac{\gamma A}{2} & -\frac{aA}{2} & 0 \\ -\frac{\sqrt{3}(a-b)}{4}\frac{\gamma A}{2} & 0 & 0 & -\frac{bA}{2} \end{pmatrix} \tag{24}$$

So finally we obtain the Floquet effective $\mathbf{k}\cdot\mathbf{p}$ Hamiltonian $\hat{H}_\Gamma^{eff}(\mathbf{k})$ as

$$\hbar v_\Gamma \eta \begin{pmatrix} ak_z & 0 & -\frac{a+3b}{4}(k_x - \frac{a\gamma v_\Gamma \eta A^2}{\Omega} + ik_y) & \frac{\sqrt{3}(a-b)}{4}(k_x - \frac{a\gamma v_\Gamma \eta A^2}{\Omega} - ik_y) \\ 0 & bk_z & \frac{\sqrt{3}(a-b)}{4}(k_x - \frac{a\gamma v_\Gamma \eta A^2}{\Omega} - ik_y) & 0 \\ -\frac{a+3b}{4}(k_x - \frac{a\gamma v_\Gamma \eta A^2}{\Omega} - ik_y) & \frac{\sqrt{3}(a-b)}{4}(k_x - \frac{a\gamma v_\Gamma \eta A^2}{\Omega} + ik_y) & -ak_z & 0 \\ \frac{\sqrt{3}(a-b)}{4}(k_x - \frac{a\gamma v_\Gamma \eta A^2}{\Omega} + ik_y) & 0 & 0 & -bk_z \end{pmatrix} \tag{25}$$

We can conclude that for the spin-$\frac{3}{2}$ excitation along the x direction, there is a momentum shift

$$\delta_\Gamma = +\frac{a\gamma v_\Gamma \eta A^2}{\Omega} = \frac{\gamma \chi_\Gamma(\eta) A^2}{\Omega} a v_\Gamma = \Xi_\Gamma a v_\Gamma \tag{26}$$

Then we take the LH CoSi ($\eta = +1$) under the pumping of LCPL ($\gamma = +1$) as an example to plot the Floquet band structures, the results are shown in Supplementary Figure 6(a) in blue lines.

D. R point with SOC

The $\mathbf{k}\cdot\mathbf{p}$ Hamiltonian of the double spin-1 excitation at the R point [4] is just the direct sum of two Hamiltonians of the spin-1 excitation as

$$\hat{H}_{\mathrm{R}}(\mathbf{k}) = -\hbar v_{\mathrm{R}}\eta\mathbf{k}\cdot(\mathbf{J}\oplus\mathbf{J}) = -\hbar v_{\mathrm{R}}\eta \begin{pmatrix} 0 & ik_z & -ik_y \\ -ik_z & 0 & ik_x \\ ik_y & -ik_x & 0 \end{pmatrix} \oplus \begin{pmatrix} 0 & ik_z & -ik_y \\ -ik_z & 0 & ik_x \\ ik_y & -ik_x & 0 \end{pmatrix} \tag{27}$$

where $\hbar v_{\mathrm{R}} = 1$ eV·Å for simplicity. Similar to the derivation process for the spin-1 excitation, for a CPL $\mathbf{A}(t) = A_0(0, \gamma\sin\Omega t, \cos\Omega t)$ incident along the x direction, we can obtain the momentum shift along the x direction of the double spin-1 excitation as

$$\delta_{\mathrm{R}} = -\frac{\gamma v_{\mathrm{R}}\eta A^2}{2\Omega} = \frac{\gamma\chi_{\mathrm{R}}(\eta)A^2}{\Omega}\frac{v_{\mathrm{R}}}{2} = \Xi_{\mathrm{R}}\frac{v_{\mathrm{R}}}{2} \tag{28}$$

which is opposite compared to the momentum shift of the spin-3/2 excitation. We also take the LH CoSi ($\eta = +1$) under the pumping of LCPL ($\gamma = +1$) as an example to plot the Floquet band structures as shown in Supplementary Figure 6(b) in red lines.

Supplementary Note 3. UNDERSTANDING THE MOMENTUM SHIFT FROM THE VIEWPOINT OF THE LIE ALGEBRA

Herein, we will prove that in the Floquet effective $\mathbf{k}\cdot\mathbf{p}$ Hamiltonian of the topological fermions, the Floquet commutator $M=\frac{1}{\hbar\Omega}\sum_{n=1}^{\infty}\frac{1}{n}[\hat{H}_n(\mathbf{k}),\hat{H}_{-n}(\mathbf{k})]$ can be expanded by the generators of the Lie algebra $su(2)$, and the momentum shift can be comprehended from the perspective of the Lie algebra $su(2)$.

A. A brief introduction of the Lie algebra

In general, the Lie algebra g is a vector space V with a bilinear map (Lie bracket) $[\cdot,\cdot]:V\times V\to V$ and satisfies [5]:

$$\begin{aligned}&\text{Antisymmetry: } [X,Y]=-[Y,X]\\&\text{Jacobi identity: } [X,[Y,Z]]+[Y,[Z,X]]+[Z,[X,Y]]=0\end{aligned}\tag{29}$$

For instance, the three-dimensional Euclidean space R^3 is a Lie algebra, and the cross product is just its Lie bracket. Actually, the Lie algebra g can be regarded as a kind of linearization of the Lie group G, because it characterizes the local structures near the identity of the Lie group G, corresponding to the tangent space (Lie algebra $g\equiv T_eG$) of the differential manifold (Lie group G) at its identity. So once we know a representation of the Lie algebra g, we can obtain a representation of the corresponding Lie group G through an exponential mapping.

For the Lie algebra $su(N)$ with n generators ($N^2-1=n$), the Lie product can be defined by

$$[X_a,X_b]=i\sum_c f_{ab}^c X_c\tag{30}$$

where the subscripts $a,b,c\in\{1,2,...,n\}$ and f_{ab}^c is the structure constant. Especially, for the Lie algebra $su(2)$, there are three generators in the space $\text{span}(X_a,X_b,X_c)$ that satisfy $[X_a,X_b]=if_{ab}^cX_c$. And the irreducible representations $X^{(S)}$ of $su(2)$ is labelled by S (spin), shown as

S	0	$\frac{1}{2}$	1	$\frac{3}{2}$	$\dots$
$\dim=2S+1$	1	2	3	4	$\dots$

B. The relationship between the Floquet commutator and the Lie algebra $su(2)$

For the topological fermions in the main text: Weyl (spin-1/2) fermion, spin-1 and spin-3/2 (Rarita-Schwinger-Weyl) excitations, their effective $\mathbf{k}\cdot\mathbf{p}$ Hamiltonians in equilibrium $\hat{H}_0(\mathbf{k})$ can all be written as $\sum_\alpha\zeta_\alpha(\mathbf{k})X_\alpha$, where X_α are the generators in the 2-, 3-, and 4-dimensional matrix irreducible representations of the Lie algebra $su(2)$, corresponding to $S=\frac{1}{2},1,\frac{3}{2}$. Moreover, the matrix elements in $\hat{H}_0(\mathbf{k})$ are all in the first order for $\mathbf{k}$, so the time-dependent $\mathbf{k}\cdot\mathbf{p}$ Hamiltonian $\hat{H}(\mathbf{k},t)$ can be decomposed as $\hat{H}_0(\mathbf{k})+\hat{H}(t)$. Because $\frac{1}{T}\int_0^T e^{\pm in\Omega t}\hat{H}_0(\mathbf{k})=0$, the Floquet commutator

M can be expressed as

$$\begin{aligned} M &= \frac{1}{\hbar\Omega}\sum_{n=1}^{\infty}\frac{1}{n}\left[\hat{H}_n(\mathbf{k}),\hat{H}_{-n}(\mathbf{k})\right] \\ &= \frac{1}{\hbar\Omega}\sum_{n=1}^{\infty}\frac{1}{n}\left[\frac{1}{T}\int_0^T e^{-in\Omega t}\hat{H}(\mathbf{k},t)dt,\frac{1}{T}\int_0^T e^{in\Omega t}\hat{H}(\mathbf{k},t)dt\right] \\ &= \frac{1}{\hbar\Omega}\sum_{n=1}^{\infty}\frac{1}{n}\left[\frac{1}{T}\int_0^T e^{-in\Omega t}\left(\hat{H}_0(\mathbf{k})+\hat{H}(t)\right)dt,\frac{1}{T}\int_0^T e^{in\Omega t}\left(\hat{H}_0(\mathbf{k})+\hat{H}(t)\right)dt\right] \\ &= \frac{1}{\hbar\Omega}\sum_{n=1}^{\infty}\frac{1}{n}\left[\frac{1}{T}\int_0^T e^{-in\Omega t}\hat{H}(t)dt,\frac{1}{T}\int_0^T e^{in\Omega t}\hat{H}(t)dt\right] \end{aligned} \tag{31}$$

It is easy to notice that $\hat{H}(t)$ can also be expanded by the generators of the Lie algebra $su(2)$ as $\sum_\alpha \zeta_\alpha(t)X_\alpha$ ($\alpha\in\{a,b,c\}$), because it is constructed by the Peierls substitution from $\hat{H}_0(\mathbf{k})$. Then

$$\begin{aligned} M &= \frac{1}{\hbar\Omega}\sum_{n=1}^{\infty}\frac{1}{n}\left[\frac{1}{T}\int_0^T e^{-in\Omega t}\hat{H}(t)dt,\frac{1}{T}\int_0^T e^{in\Omega t}\hat{H}(t)dt\right] \\ &= \frac{1}{\hbar\Omega}\sum_{n=1}^{\infty}\frac{1}{n}\left[\frac{1}{T}\int_0^T e^{-in\Omega t}\left(\sum_\alpha\zeta_\alpha(t)X_\alpha\right)dt,\frac{1}{T}\int_0^T e^{in\Omega t}\left(\sum_\beta\zeta_\beta(t)X_\beta\right)dt\right] \\ &= \frac{1}{\hbar\Omega}\sum_{n=1}^{\infty}\frac{1}{n}\left[\sum_\alpha\zeta_{\alpha,-n}X_\alpha,\sum_\beta\zeta_{\beta,n}X_\beta\right] \\ &= \frac{1}{\hbar\Omega}\sum_{n=1}^{\infty}\frac{1}{n}\sum_\alpha\sum_\beta\zeta_{\alpha,-n}\zeta_{\beta,n}\left[X_\alpha,X_\beta\right] \\ &= \frac{i}{\hbar\Omega}\sum_{n=1}^{\infty}\frac{1}{n}\sum_\alpha\sum_\beta\zeta_{\alpha,-n}\zeta_{\beta,n}f^k_{\alpha\beta}X_k \end{aligned} \tag{32}$$

where we have defined $\zeta_{\alpha,\pm n}=\frac{1}{T}\int_0^T e^{\pm in\Omega t}\zeta_\alpha(t)dt$. We can see from Supplementary Equation 32 that the Floquet commutator M can still be expanded by the generators of the Lie algebra $su(2)$.

C. The LPL pumping case

We should emphasize that, for the LPL pumping, regardless of the polarization direction, the phase of the component along the a (b,c) direction remains constant.

If the polarization direction of the pumping light is along the a (b,c) direction, there is only a single direction for the Peierls substitution ($k_\alpha\to k_\alpha+A\sin\Omega t$), leading to $\hat{H}(t)=\zeta_\alpha(t)X_\alpha$. Consequently, the Floquet commutator M must be zero due to $[X_\alpha,X_\alpha]=0$, implying that topological fermions do not exhibit no momentum shifts under the LPL pumping in the framework of the Floquet engineering.

For the more general case, we can write down the general form of the vector potential for the LPL as $\mathbf{A}(t)=\cos\Omega t(A_a,A_b,A_c)$. Then we can derive the Floquet commutator M in Supplementary Equation 32 as:

$$
\begin{aligned}
M &= \frac{1}{\hbar\Omega}\sum_{n=1}^{\infty}\frac{1}{n}\left[\frac{1}{T}\int_0^T e^{-in\Omega t}\hat{H}(t)dt, \frac{1}{T}\int_0^T e^{in\Omega t}\hat{H}(t)dt\right] \\
&= \frac{1}{\hbar\Omega}\sum_{n=1}^{\infty}\frac{1}{n}\left[\frac{1}{T}\int_0^T e^{-in\Omega t}\left(\sum_{\alpha}\zeta_{\alpha}(t)X_{\alpha}\right)dt, \frac{1}{T}\int_0^T e^{in\Omega t}\left(\sum_{\beta}\zeta_{\beta}(t)X_{\beta}\right)dt\right] \\
&= \frac{1}{\hbar\Omega}\sum_{n=1}^{\infty}\frac{1}{n}\left[\frac{1}{T}\int_0^T e^{-in\Omega t}\left(\sum_{\alpha}\zeta(t)A_{\alpha}X_{\alpha}\right)dt, \frac{1}{T}\int_0^T e^{in\Omega t}\left(\sum_{\beta}\zeta(t)A_{\beta}X_{\beta}\right)dt\right] \\
&= \frac{1}{\hbar\Omega}\sum_{n=1}^{\infty}\frac{1}{n}\zeta_{-n}\zeta_{n}\left[\sum_{\alpha}A_{\alpha}X_{\alpha}, \sum_{\beta}A_{\beta}X_{\beta}\right]
\end{aligned}
\tag{33}
$$

where A_α is the time-independent component of the vector potential $\mathbf{A}(t)$ along the α direction and we have defined $\zeta_{\pm n} = \frac{1}{T}\int_0^T e^{\pm in\Omega t}\zeta(t)dt$. Notice that $\alpha, \beta \in \{a, b, c\}$, $\left[\sum_\alpha A_\alpha X_\alpha, \sum_\beta A_\beta X_\beta\right]$ must be zero.

For clarity, let's consider a straightforward example. Suppose the polarization direction of the vector potential lies in the xy plane, as shown in the inset of Supplementary Figure 7(c), we can then write down the vector potential for the LPL as $\mathbf{A}(t) = A\cos\Omega t(\sin\theta, \cos\theta, 0)$, where A is the amplitude of the vector potential. In this case, $\alpha, \beta \in \{x, y\}$, and we can derive the Floquet commutator M as:

$$
\begin{aligned}
M &= \frac{1}{\hbar\Omega}\sum_{n=1}^{\infty}\frac{1}{n}\zeta_{-n}\zeta_{n}\left[\sum_{\alpha}A_{\alpha}X_{\alpha}, \sum_{\beta}A_{\beta}X_{\beta}\right] \\
&= \frac{1}{\hbar\Omega}\sum_{n=1}^{\infty}\frac{1}{n}\zeta_{-n}\zeta_{n}\left[A_xX_x + A_yX_y, A_xX_x + A_yX_y\right] \\
&= \frac{1}{\hbar\Omega}\sum_{n=1}^{\infty}\frac{1}{n}\zeta_{-n}\zeta_{n}A^2\left[\sin\theta X_x + \cos\theta X_y, \sin\theta X_x + \cos\theta X_y\right] \\
&= 0
\end{aligned}
\tag{34}
$$

We also perform the Floquet tight-binding calculations for spin-1 and double Weyl fermions, as illustrated in Supplementary Figure 7(c) and Supplementary Figure 7(d). Therefore, in general, in the framework of the Floquet engineering, upon the LPL pumping, there are no momentum shifts regardless of the polarization direction.

D. The CPL pumping case

But for the CPL pumping, the situation is different. Because there are at least two directions for the Peierls substitution ($k_\alpha \to k_\alpha + \gamma A\sin\Omega t$ and $k_\beta \to k_\beta + A\cos\Omega t$), we can obtain the Floquet commutator as

$$
\begin{aligned}
M &\simeq \left[\frac{1}{T}\int_0^T e^{-in\Omega t}\hat{H}(t)dt, \frac{1}{T}\int_0^T e^{in\Omega t}\hat{H}(t)dt\right] \\
&= \left[\zeta_{\alpha,-n}X_\alpha + \zeta_{\beta,-n}X_\beta, \zeta_{\alpha,n}X_\alpha + \zeta_{\beta,n}X_\beta\right] \\
&= (\zeta_{\alpha,-n}\zeta_{\beta,n} - \zeta_{\alpha,n}\zeta_{\beta,-n})[X_\alpha, X_\beta] \\
&= i\zeta^n_{\alpha\beta}f^k_{\alpha\beta}X_k
\end{aligned}
\tag{35}
$$

where $(\zeta_{\alpha,-n}\zeta_{\beta,n}-\zeta_{\alpha,n}\zeta_{\beta,-n})\neq 0$ has been rewritten as $\zeta^n_{\alpha\beta}$ for simplicity. We can see the Floquet commutator M is nonzero, and X_k just corresponds to the third generator. This indicates that the shift is along the k direction, which aligns with the propogation direction of the CPL. So finally under the illumination of CPL, there is a momentum shift instead of the splitting for topological fermions.

Furthermore, for double Weyl and double spin-1 fermions, their effective $\mathbf{k}\cdot\mathbf{p}$ Hamiltonians in equilibrium are just the direct sum of two Weyl fermions and two spin-1 fermions with the same chirality, which corresponds to totally reducible representations of the Lie algebra $su(2)$, and can be divided into the direct sum of two irreducible representations. Using methods similar to the above, we can demonstrate the CPL-induced Floquet commutator $M\simeq i\zeta^n_{\alpha\beta}f^k_{\alpha\beta}(X_k\oplus X_k)$, which also denotes a momentum shift.

As for the opposite momentum shifts for spin-1 and double Weyl fermions shown in the main text, the fundamental reason is that the structure constants f^c_{ab} of their Lie algebra $su(2)$ are opposite numbers. For the spin-1 excitation $\hat{H}_\Gamma(\mathbf{k})=\hbar v_\Gamma\eta\mathbf{k}\cdot\mathbf{J}$, $\mathbf{J}$ is just generators of the Lie algebra $su(2)$ as

$$J_x=\begin{bmatrix}0&0&0\\0&0&\mathrm{i}\\0&-\mathrm{i}&0\end{bmatrix},J_y=\begin{bmatrix}0&0&-\mathrm{i}\\0&0&0\\\mathrm{i}&0&0\end{bmatrix},J_z=\begin{bmatrix}0&\mathrm{i}&0\\-\mathrm{i}&0&0\\0&0&0\end{bmatrix} \tag{36}$$

and satisfies $[J_a,J_b]=if^c_{ab}J_c=-i\epsilon^c_{ab}J_c$, where ϵ^c_{ab} is the Levi-Civita symbol. For the convenience of the following analysis, we can redefine $\tilde{J}_i=2J_i$, then $[\tilde{J}_a,\tilde{J}_b]=-2i\epsilon^c_{ab}\tilde{J}_c$. From Supplementary Equation 35 we can obtain the CPL-induced Floquet commutator M as

$$M\simeq i\zeta^n_{\alpha\beta}f^k_{\alpha\beta}X_k=i\zeta^n_{\alpha\beta}f^k_{\alpha\beta}J_k=-2i\zeta^n_{\alpha\beta}\epsilon^k_{\alpha\beta}(\frac{1}{4}\tilde{J}_k) \tag{37}$$

But for the double Weyl fermion $\hat{H}_R(\mathbf{k})=\hbar v_R\eta\mathbf{k}\cdot(\boldsymbol{\sigma}\oplus\boldsymbol{\sigma})$, as generators of the Lie algebra $su(2)$, $\boldsymbol{\sigma}$ satisfies $[\sigma_a,\sigma_b]=if^c_{ab}\sigma_c=2i\epsilon^c_{ab}\sigma_c$, then the CPL-induced Floquet commutator M can be expressed as

$$M\simeq i\zeta^n_{\alpha\beta}f^k_{\alpha\beta}(X_k\oplus X_k)=2i\zeta^n_{\alpha\beta}\epsilon^k_{\alpha\beta}(\sigma_k\oplus\sigma_k) \tag{38}$$

Herein from Supplementary Equation 37 and Supplementary Equation 38 we can ascertain that the opposite momentum shifts stem from the opposite structure constants.

However, for the Dirac fermion $\hat{H}_D(\mathbf{k})=\mathbf{k}\cdot(\boldsymbol{\sigma}\oplus\boldsymbol{\sigma}^*)$, $\boldsymbol{\sigma}$ and $\boldsymbol{\sigma}^*$ satisfy different Lie products: $[\sigma_a,\sigma_b]=2i\epsilon^c_{ab}\sigma_c$ and $[\sigma^*_a,\sigma^*_b]=-2i\epsilon^c_{ab}\sigma^*_c$, so the Lie product of $\boldsymbol{\sigma}\oplus\boldsymbol{\sigma}^*$ is not closed (for instance, $[\sigma_1\oplus\sigma^*_1,\sigma_2\oplus\sigma^*_2]=[\sigma_1,\sigma_2]\oplus[\sigma^*_1,\sigma^*_2]=2i\sigma_3\oplus(-2i\sigma^*_3)=2i\{\sigma_3\oplus(-\sigma_3)\}$ cannot be expanded by $\sigma_3\oplus\sigma^*_3=\sigma_3\oplus\sigma_3$). Then we can follow the similar derivation process as above and obtain the CPL-induced Floquet commutator $M\simeq 2i\zeta^n_{\alpha\beta}\epsilon^k_{\alpha\beta}\{\sigma_k\oplus(-\sigma^*_k)\}$. The minus sign indicates that the Dirac fermion will split up into two Weyl fermions, which will shift along opposite directions.

Furthermore, we can give a general description from the viewpoint of the quantum field theory (QFT). Actually, the Dirac fermion (spinor) is just the reducible representation of the Lorentz algebra $so(1,3)\simeq su(2)\otimes su(2)$. Once we know all (irreducible) representations of the Lie algebra $su(2)$, we can obtain all (irreducible) representations of the Lorentz algebra $so(1,3)$. We can label each irreducible representation with (S_+,S_-), and the corresponding dimension of the irreducible representation is just $(2S_++1)(2S_-+1)$. For example, the left- and right-handed Weyl fermions (spinors) can be denoted as $(\frac{1}{2},0)$ and $(0,\frac{1}{2})$, and the Dirac fermion (spinor) is a combination of two Weyl fermions (spinors) with opposite chirality, represented as $(\frac{1}{2},0)\oplus(0,\frac{1}{2})$, aligning with the earlier analysis.

More generally, our results are not limited to the topological fermions in this work. Some other spin-S topological excitations [6] have been observed in the universe of solids due to the space group symmetry restrictions, which are less stringent compared to the Poincaré symmetry in the field of the high energy physics. For the spin-S topological excitations, there also could be CPL-induced momentum shifts in the framework of the Floquet engineering.

Supplementary Note 4. FLOQUET TIGHT-BINDING HAMILTONIAN

A. The LPL-induced Floquet band structures of the CoSi compound

In Methods in the main text we have constructed the matrix element of the Floquet tight-binding Hamiltonian as $\hat{\mathcal{H}}_{nm}(\mathbf{k}) = \frac{1}{T}\int_0^T dt \hat{H}^{TB}(\mathbf{k},t)e^{i(n-m)\Omega t} - m\hbar\Omega\delta_{mn}$, where m, n are Floquet indices. To confirm the absence of momentum shifts for topological fermions under the LPL pumping, we choose the LH CoSi without SOC as a case study to calculate Floquet band structures. First, we define the LPL as $\mathbf{A}(t) = A_0(\sin\Omega t, 0, 0)$, maintaining the same pumping photon energy $\hbar\Omega$ and electric field intensity $A_0\Omega$ as in the main text. As depicted in Supplementary Figure 7(a) and Supplementary Figure 7(b), for both spin-1 and double Weyl fermions, no momentum shifts are observed.

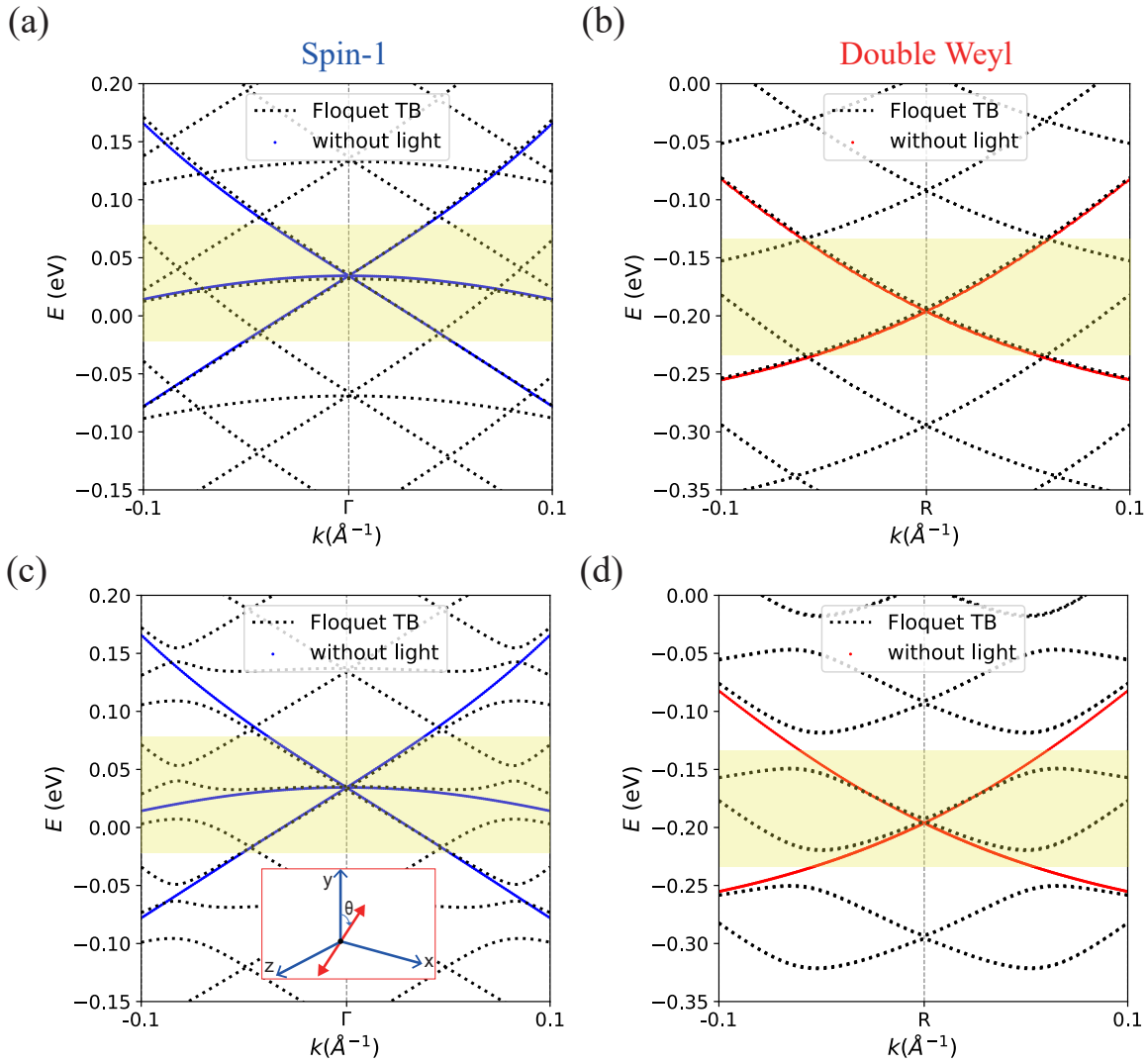

Supplementary Figure 7. (a) Band structures without light pumping in blue dot lines and Floquet band structures upon the LPL radiation from the diagonalization of the Floquet tight-binding Hamiltonian in black dashed lines for the spin-1 excitation around the Γ point without SOC. (b) Analogous results to (a) but for the double Weyl fermion around the R point. The band structures without light pumping are denoted in red dot lines. (c,d) Analogous results to (a,b) but for a more general LPL. The inset in (c) illustrates the polarization direction of the LPL at $\theta = 30°$ during the calculations of this part. The shaded yellow regions represent the first Floquet-Brillouin zone (FBZ) in $[-\frac{\hbar\Omega}{2}, \frac{\hbar\Omega}{2})$. The truncation of m and n indices is set to $\{-2, -1, 0, 1, 2\}$.

For a more general case, we select the vector potential of the LPL in the xy plane as $\mathbf{A}(t) = A_0(\sin\theta\sin\Omega t, \cos\theta\sin\Omega t, 0) = A_0\sin\Omega t(\sin\theta, \cos\theta, 0)$, as shown in the inset of Supplementary Figure 7(c). But still, as depicted in Supplementary Figure 7(c) and Supplementary Figure 7(d), for both spin-1 and double Weyl fermions, no momentum shifts are observed, which validates our previous analysis based on the Floquet effective $\mathbf{k}\cdot\mathbf{p}$ Hamiltonian in Supplementary Note 2 A and the Lie algebra $su(2)$ in Supplementary Note 3.

B. The LCPL-induced Floquet band structures of CoSi and AlPt compounds

Regarding the LCPL pumping laser for the LH CoSi crystal, in the main text without SOC, we choose the truncation of m and n indices as $\{-1, 0, 1\}$. The results of the truncation as $\{-2, -1, 0, 1, 2\}$ are presented in Supplementary Figure 8 with the same photon energy and electric field intensity. The truncation used in this work is sufficient to describe the momentum shifts of the topological fermions.

For the AlPt compound, because of effects from the heavy element Pt, we should consider SOC in the calculations of Floquet band structures. The results are shown in Supplementary Figure 9 and the truncations of m and n are $\{-2, -1, 0, 1, 2\}$. We should point out that, for the spin-3/2 and double spin-1 fermions under the laser pumping in the framework of the Floquet engineering, in order to decrease the effects of bands (pointed by blue and red arrows in Supplementary Figure 9(a) and Supplementary Figure 9(b)) closer to them, we choose the pumping photon energy as 320 meV and the electric field intensity as 5.4×10^7 V/m, which also shows the adjustability of the parameters to induce the momentum shift. But actually, the degeneracy of these crossing points is not very perfect as shown in the insets in the upper right corner of Supplementary Figure 9(a) and Supplementary Figure 9(b). This is related to the fit quality of the Wannier functions, which are the fundamental of the Floquet tight-binding Hamiltonian. But the characteristic of momentum shift still exists, which is also confirmed by Floquet effective $\mathbf{k}\cdot\mathbf{p}$ Hamiltonians in Supplementary Note 2 C and Supplementary Note 2 D.

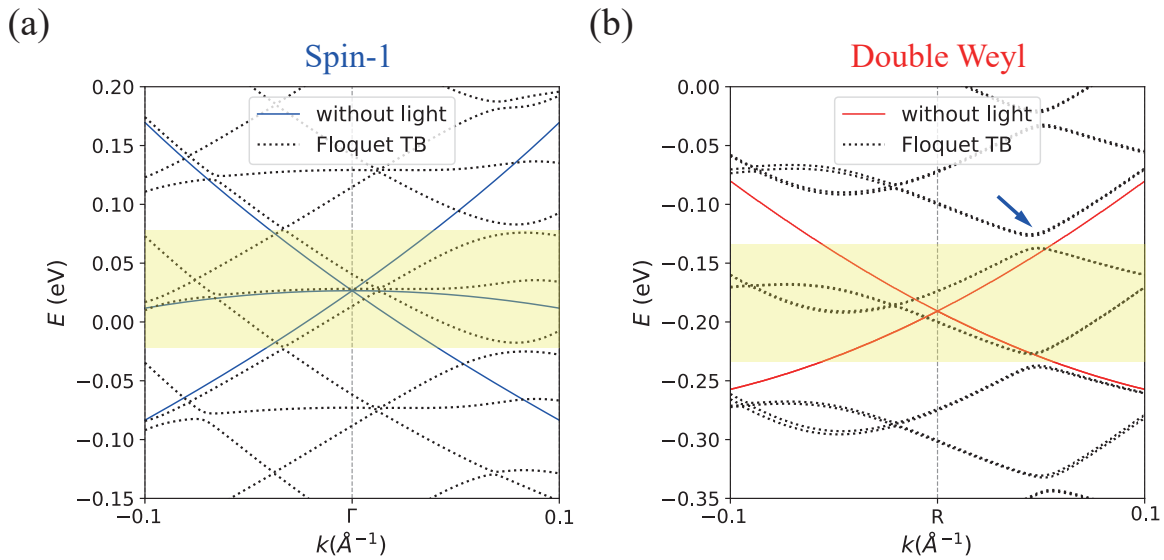

Supplementary Figure 8. (a) Band structures without light pumping in blue lines and Floquet band structures upon the LCPL radiation from the diagonalization of the Floquet tight-binding Hamiltonian in black dot lines for the spin-1 excitation around the Γ point without SOC. (b) Analogous results to (a) but for the double Weyl fermion around the R point. The band structures without light pumping are denoted in red lines. All results are calculated for the LH CoSi crystal. The shaded yellow regions represent the first FBZ in $[-\frac{\hbar\Omega}{2}, \frac{\hbar\Omega}{2})$.

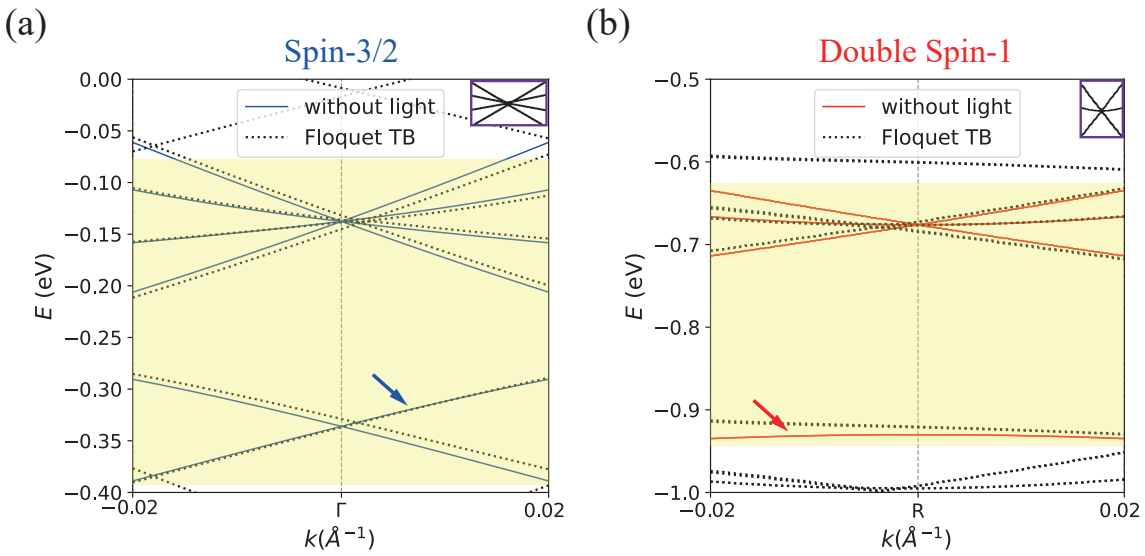

Supplementary Figure 9. (a) Band structures without light pumping in blue lines and Floquet band structures upon the LCPL radiation from the diagonalization of the Floquet tight-binding Hamiltonian in black dot lines for the spin-3/2 excitation around the Γ point with SOC. (b) Analogous results to (a) but for the double spin-1 fermion around the R point. The band structures without light pumping are denoted in red lines. All results are calculated for the LH AlPt crystal. The shaded yellow regions represent the first FBZ in $[-\frac{\hbar\Omega}{2}, \frac{\hbar\Omega}{2})$.

C. The LCPL-induced Fermi arc states on the (001) surface with SOC

When we consider the effects of SOC, the Fermi arc states on the (001) surface for the LH and RH CoSi at the zero-energy cut can also be calculated as shown in Supplementary Figure 10. We observe the release of degeneracy in the light-induced surface states, yet their connections persist in alignment with the scenario without SOC under the light pumping in the main text. We choose the pumping photon energy as 100 meV and the electric field intensity as 4.4×10^7 V/m during CoSi calculations.

As for the LH and RH AlPt, we show corresponding results in Supplementary Figure 11 with the pumping photon energy as 320 meV and the electric field intensity as 5.4×10^7 V/m.

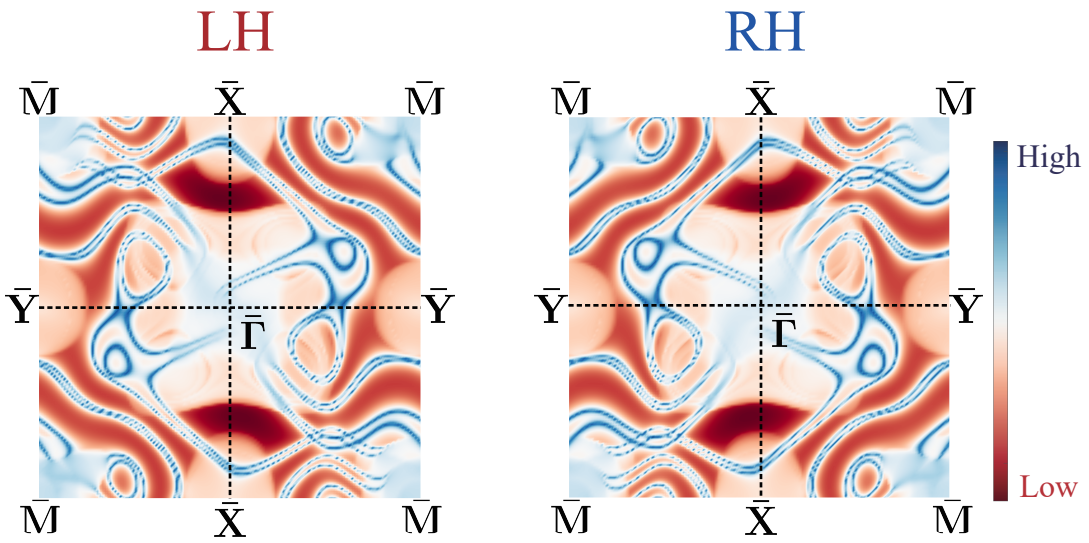

Supplementary Figure 10. The schematic of the Fermi arc states on the (001) surface for the LH (left panel) and RH (right panel) CoSi at the zero-energy cut when SOC is included upon the irradiation of the LCPL.

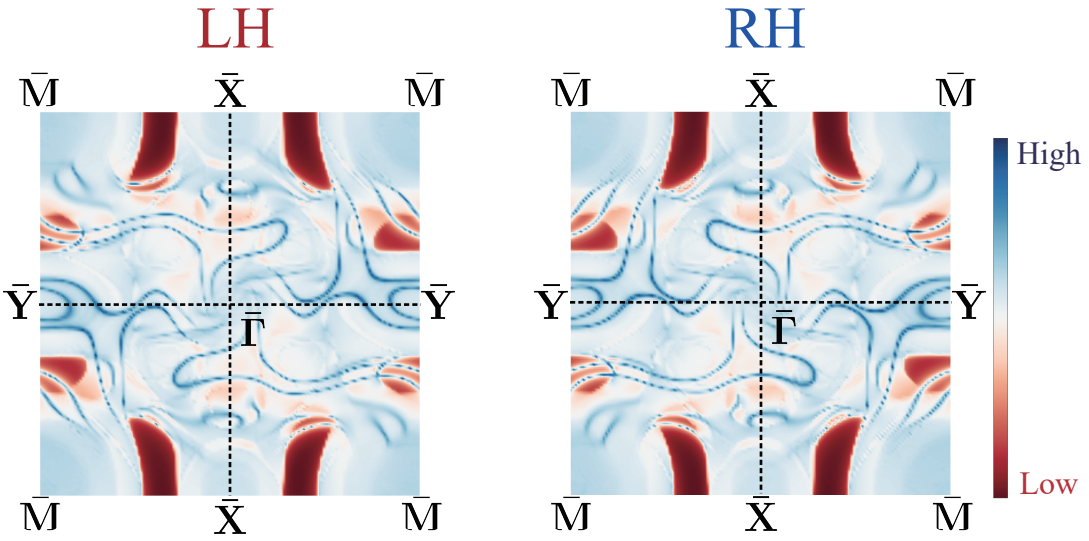

Supplementary Figure 11. The schematic of the Fermi arc states on the (001) surface for the LH (left panel) and RH (right panel) AlPt at the zero-energy cut when SOC is included upon the irradiation of the LCPL.

Supplementary Note 5. VALIDITY OF THE HIGH-FREQUENCY LIMIT

In Supplementary Note 2, we construct the Floquet effective $\mathbf{k}\cdot\mathbf{p}$ Hamiltonians for topological fermions at Γ and R points without and with SOC to investigate the light-matter interactions. A complementary approach to show the validity of the high-frequency limit is to calculate the Floquet band structures obtained from the diagonalization of the Floquet extended $\mathbf{k}\cdot\mathbf{p}$ Hamiltonian and compare them with the results from the Floquet effective $\mathbf{k}\cdot\mathbf{p}$ Hamiltonian. Herein, we take the double Weyl fermion at the R point without SOC as a starting point. Actually, as shown in Supplementary Equation 14, the double Weyl fermion is the direct sum of two Weyl fermions with the same topological charge, so without loss of generality, we can analyze the Weyl fermion to clarify this issue.

The effective $\mathbf{k}\cdot\mathbf{p}$ Hamiltonian of the Weyl fermion is expressed as

$$\hat{H}_W(\mathbf{k}) = \hbar v_W \eta \mathbf{k}\cdot\boldsymbol{\sigma} = \hbar v_W \eta \begin{pmatrix} k_z & k_x - ik_y \\ k_x + ik_y & -k_z \end{pmatrix} \tag{39}$$

where we set $\hbar v_W = 0.88$ eV·Å. For the convenience of the next analysis and discussion, we perform a unitary transformation to the matrix in Supplementary Equation 39 as

$$\begin{aligned} \hat{H}_W(\mathbf{k}) &= \hbar v_W \eta \begin{pmatrix} -\frac{1}{\sqrt{2}} & \frac{1}{\sqrt{2}} \\ \frac{1}{\sqrt{2}} & \frac{1}{\sqrt{2}} \end{pmatrix} \begin{pmatrix} k_z & k_x - ik_y \\ k_x + ik_y & -k_z \end{pmatrix} \begin{pmatrix} -\frac{1}{\sqrt{2}} & \frac{1}{\sqrt{2}} \\ \frac{1}{\sqrt{2}} & \frac{1}{\sqrt{2}} \end{pmatrix} \\ &= \hbar v_W \eta \begin{pmatrix} -k_x & -k_z + ik_y \\ -k_z - ik_y & k_x \end{pmatrix} \end{aligned} \tag{40}$$

Such a unitary transformation does not change the topological charge of the Weyl fermion. Then we consider a CPL represented as $\mathbf{A}(t) = A_0(0, \gamma \sin\Omega t, \cos\Omega t)$ incident along the x direction, where $\gamma = \pm 1$ denotes LCPL and RCPL. By applying the Peierls substitution $k_y \to k_y + \gamma \frac{eA_0}{\hbar}\sin\Omega t$ and $k_z \to k_z + \frac{eA_0}{\hbar}\cos\Omega t$, the time-dependent $\mathbf{k}\cdot\mathbf{p}$ Hamiltonian for CPL is obtained as

$$\hat{H}_W^F(\mathbf{k}, t) = \hbar v_W \eta \begin{pmatrix} -k_x & -k_z + ik_y + A(-\cos\Omega t + i\gamma \sin\Omega t) \\ -k_z - ik_y + A(-\cos\Omega t - i\gamma\sin\Omega t) & k_x \end{pmatrix} \tag{41}$$

where we have redefined $A = \frac{eA_0}{\hbar}$ for simplicity. Then, consistent with the discussion in Supplementary Note 2 B, we employ the Floquet theory to obtain the time-independent Floquet matrix elements as

$$\begin{aligned} \left[\hat{H}_W^F(\mathbf{k})\right]_{nm} &= \frac{1}{T}\int_0^T dt \hat{H}_W^F(\mathbf{k}, t) e^{i(n-m)\Omega t} - m\hbar\Omega\delta_{mn} \\ &= \begin{pmatrix} (-k_x - m\hbar\Omega)\delta_{mn} & (-k_z + ik_y)\delta_{mn} + \frac{A}{2}(-\delta_{m,n+1} - \delta_{m,n-1} + \gamma\delta_{m,n+1} - \gamma\delta_{m,n-1}) \\ (-k_z - ik_y)\delta_{mn} + \frac{A}{2}(-\delta_{m,n+1} - \delta_{m,n-1} - \gamma\delta_{m,n+1} + \gamma\delta_{m,n-1}) & (k_x - m\hbar\Omega)\delta_{mn} \end{pmatrix} \end{aligned} \tag{42}$$

where $T = 2\pi/\Omega$ is one optical cycle of the pumping laser and we omit $\hbar v_W \eta$ for simplicity. Now we only consider the first-order contributions of light-matter interaction within the framework of Floquet theory. By truncating the time-independent Floquet extended $\mathbf{k}\cdot\mathbf{p}$ Hamiltonian $\hat{H}_W^F(\mathbf{k})$ in Supplementary Equation 42 to $m, n = \{-1, 0, 1\}$, we obtain $\hat{H}_W^F(\mathbf{k})$ as

$$\hat{H}_W^F(\mathbf{k}) = \begin{pmatrix} -k_x + \hbar\Omega & -k_z + ik_y & 0 & \frac{A}{2}(\gamma - 1) & 0 & 0 \\ -k_z - ik_y & k_x + \hbar\Omega & \frac{A}{2}(-\gamma - 1) & 0 & 0 & 0 \\ 0 & \frac{A}{2}(-\gamma - 1) & -k_x & -k_z + ik_y & 0 & \frac{A}{2}(\gamma - 1) \\ \frac{A}{2}(\gamma - 1) & 0 & -k_z - ik_y & k_x & \frac{A}{2}(-\gamma - 1) & 0 \\ 0 & 0 & 0 & \frac{A}{2}(-\gamma - 1) & -k_x - \hbar\Omega & -k_z + ik_y \\ 0 & 0 & \frac{A}{2}(\gamma - 1) & 0 & -k_z - ik_y & k_x - \hbar\Omega \end{pmatrix} \tag{43}$$

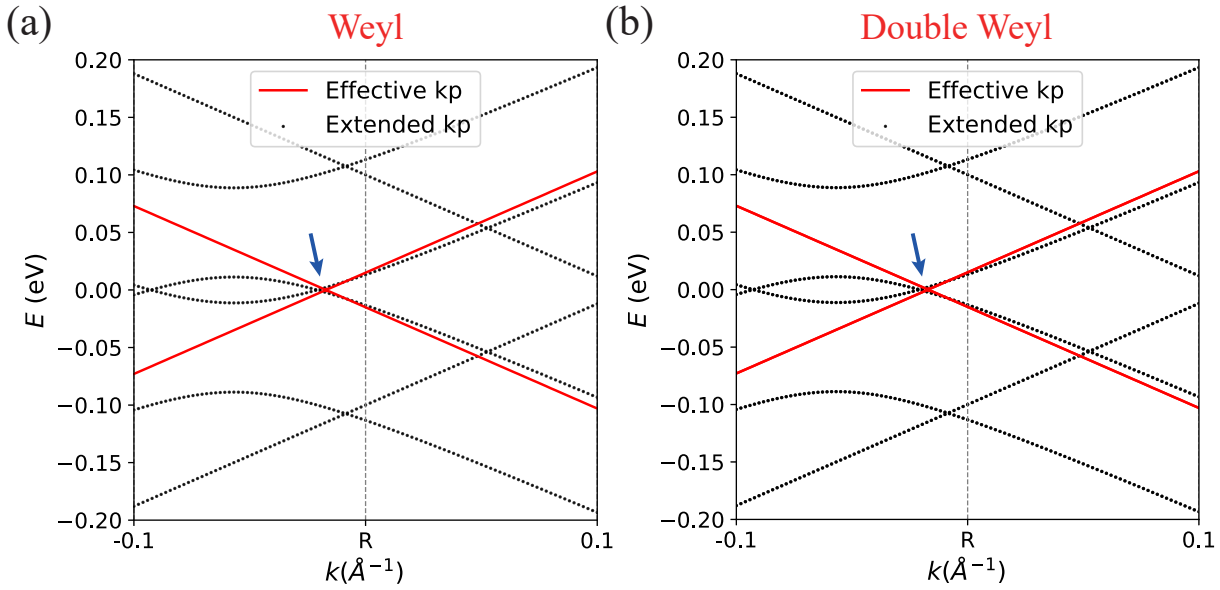

Supplementary Figure 12. (a) Floquet band structures from the Floquet extended $\mathbf{k}\cdot\mathbf{p}$ Hamiltonian in black dot lines and from the Floquet effective $\mathbf{k}\cdot\mathbf{p}$ Hamiltonian in red lines are shown for the Weyl fermion. (b) Similar results but for the double Weyl fermion.

We only focus on the Floquet band structures along the k_x direction, which is also the propagation direction of the CPL. So let $k_y = 0$ and $k_z = 0$, we obtain

$$\hat{H}_W^F(k_x) = \begin{pmatrix} -k_x+\hbar\Omega & 0 & 0 & \frac{A}{2}(\gamma-1) & 0 & 0 \\ 0 & k_x+\hbar\Omega & \frac{A}{2}(-\gamma-1) & 0 & 0 & 0 \\ 0 & \frac{A}{2}(-\gamma-1) & -k_x & 0 & 0 & \frac{A}{2}(\gamma-1) \\ \frac{A}{2}(\gamma-1) & 0 & 0 & k_x & \frac{A}{2}(-\gamma-1) & 0 \\ 0 & 0 & 0 & \frac{A}{2}(-\gamma-1) & -k_x-\hbar\Omega & 0 \\ 0 & 0 & \frac{A}{2}(\gamma-1) & 0 & 0 & k_x-\hbar\Omega \end{pmatrix} \tag{44}$$

In the same way as shown in Supplementary Note 2 B, we can also obtain the Floquet effective $\mathbf{k}\cdot\mathbf{p}$ Hamiltonian of the Weyl fermion as

$$\hat{H}_W^{eff}(\mathbf{k}) = \hbar v_W \eta \left(\mathbf{k}\cdot\boldsymbol{\sigma} + \frac{\gamma v_W \eta A^2}{\Omega}\sigma_x \right) \tag{45}$$

Now we set $\eta = +1$ and $\gamma = +1$ as an example to plot the Floquet band structures along the k_x direction from the diagonalization of the Floquet extended $\mathbf{k}\cdot\mathbf{p}$ Hamiltonian [Supplementary Equation 44] and from the Floquet effective $\mathbf{k}\cdot\mathbf{p}$ Hamiltonian [Supplementary Equation 45]. The calculated results are shown in Supplementary Figure 12(a). We can see, to some extent, the Floquet effective $\mathbf{k}\cdot\mathbf{p}$ Hamiltonian can capture the key feature of the light-matter interaction for the Weyl fermion, such as the momentum shift highlighted by the blue arrow in Supplementary Figure 12(a). So the high-frequency limit used in the main text is reliable. In addition, we also calculate the corresponding results for the double Weyl fermion in Supplementary Figure 12(b), and ensure that the analysis of the Weyl fermion can also be applied to the double Weyl fermion because their Floquet quasienergy spectra are the same.

Moreover, Some new features in Floquet band structures can be found beyond the Floquet effective $\mathbf{k}\cdot\mathbf{p}$ Hamiltonian for the Weyl fermion, as shown in Supplementary Figure 13(a). Two red Floquet bands have a hybridization with a gap instead of a crossing, but two blue Floquet bands keep the

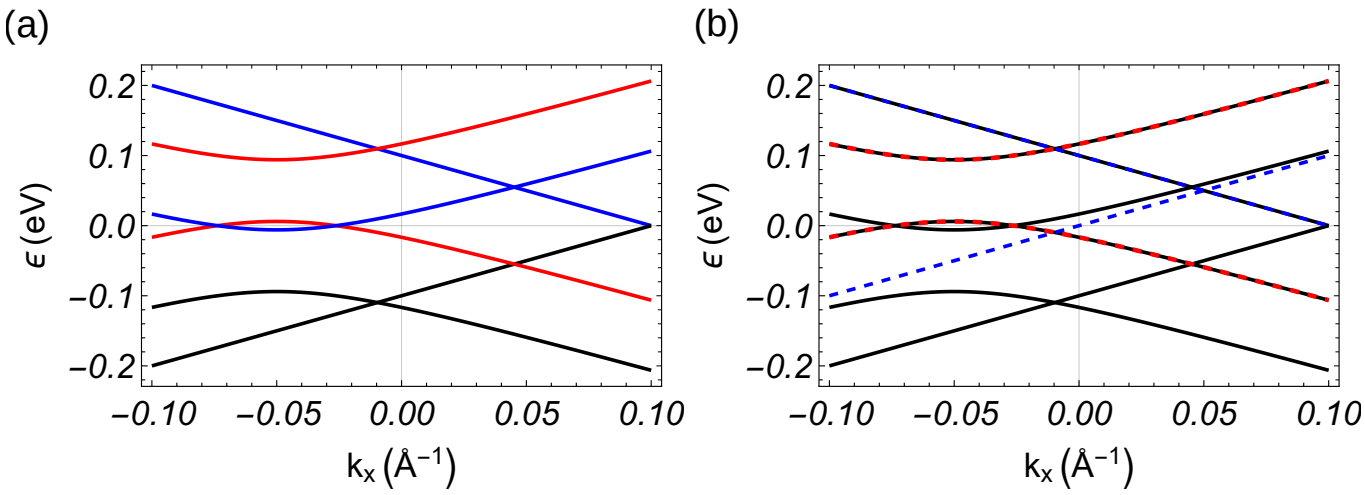

Supplementary Figure 13. (a) Floquet band structures from the Floquet extended $\mathbf{k}\cdot\mathbf{p}$ Hamiltonian $\hat{H}_W^F(k_x)$ are shown for the Weyl fermion. The red and blue Floquet bands are what we are concerned about. (b) Floquet band structures are shown in black lines. The Floquet bands in red and blue dot lines are obtained from the diagonalization of $\hat{H}_1(k_x)$ and $\hat{H}_2(k_x)$ in Supplementary Equation 48, respectively.

band crossing. Such phenomena are related to the interactions between Floquet bands with different Floquet indices of $m, n = -1$ and $m, n = 0$.

To provide an intuitive physical picture, we can directly pick up the four-band Hamiltonian from the Floquet extended $\mathbf{k}\cdot\mathbf{p}$ Hamiltonian $\hat{H}_W^F(k_x)$ in Supplementary Equation 44 as

$$\hat{H}_W^{4\times4}(k_x) = \begin{pmatrix} -k_x+\hbar\Omega & 0 & 0 & \frac{A}{2}(\gamma-1) \\ 0 & k_x+\hbar\Omega & \frac{A}{2}(-\gamma-1) & 0 \\ 0 & \frac{A}{2}(-\gamma-1) & -k_x & 0 \\ \frac{A}{2}(\gamma-1) & 0 & 0 & k_x \end{pmatrix} \tag{46}$$

We then rearrange the matrix elements in the $\hat{H}_W^{4\times4}(k_x)$ as

$$\hat{H}_W^{4\times4}(k_x) = \begin{pmatrix} k_x+\hbar\Omega & \frac{A}{2}(-\gamma-1) & 0 & 0 \\ \frac{A}{2}(-\gamma-1) & -k_x & 0 & 0 \\ 0 & 0 & k_x & \frac{A}{2}(\gamma-1) \\ 0 & 0 & \frac{A}{2}(\gamma-1) & -k_x+\hbar\Omega \end{pmatrix} \tag{47}$$

Let $\gamma = +1$, we obtain

$$\begin{aligned} \hat{H}_W^{4\times4}(k_x) &= \begin{pmatrix} k_x+\hbar\Omega & -A & 0 & 0 \\ -A & -k_x & 0 & 0 \\ 0 & 0 & k_x & 0 \\ 0 & 0 & 0 & -k_x+\hbar\Omega \end{pmatrix} \\ &= \begin{pmatrix} k_x+\hbar\Omega & -A \\ -A & -k_x \end{pmatrix} \oplus \begin{pmatrix} k_x & 0 \\ 0 & -k_x+\hbar\Omega \end{pmatrix} \\ &= \hat{H}_1(k_x) \oplus \hat{H}_2(k_x) \end{aligned} \tag{48}$$

We can diagonalize the reduced Hamiltonians $\hat{H}_1(k_x)$ and $\hat{H}_2(k_x)$ in Supplementary Equation 48, and the results are shown in Supplementary Figure 13(b). The red dashed lines are from the reduced

Hamiltonians $\hat{H}_1(k_x)$ and the blue dashed lines are from the reduced Hamiltonians $\hat{H}_2(k_x)$. Because the off-diagonal term in the reduced Hamiltonians $\hat{H}_1(k_x)$ is $-A$, which is nonzero, two red bands will decouple and have a gap between them. Conversely, the off-diagonal term in the reduced Hamiltonians $\hat{H}_2(k_x)$ is 0, so two blue bands will have a crossing point. In a word, the chirality of the CPL can affect the coupling between Floquet bands with different Floquet index.

In addition, if we compare the Floquet band structures of the double Weyl fermion from the Floquet tight-binding Hamiltonian shown in Supplementary Figure 8(b) and from the Floquet extended $\mathbf{k}\cdot\mathbf{p}$ Hamiltonian shown in Supplementary Figure 12(b), we can see in Supplementary Figure 8(b), the Floquet bands pointed by the blue arrow also have a gap, which does not match the analysis above (two blue Floquet bands have a crossing point instead of a gap in Supplementary Figure 13(a)).

Actually, the above discussion is based on the fact that matrix elements in the effective $\mathbf{k}\cdot\mathbf{p}$ Hamiltonian of the Weyl fermion are all in the first order for $\mathbf{k}$, so the reduced Hamiltonian $\hat{H}_2(k_x)$ in Supplementary Equation 48 possesses zero off-diagnal terms. If high order terms for $\mathbf{k}$ are considered in the effective $\mathbf{k}\cdot\mathbf{p}$ Hamiltonian, some nonzero off-diagnal terms will emerge in the reduced Hamiltonian $\hat{H}_2(k_x)$, and the gap will occur between two blue Floquet bands, which has been captured by the calculations of the Floquet tight-binding Hamiltonian.

Supplementary Note 6. THE ESTIMATION OF THE SCATTERING TIME IN COSI SINGLE CRYSTAL

In different growth conditions of the CoSi single crystal, the estimated mobility μ_e is around $2.3 \times 10^2 \sim 7.3 \times 10^3$ $\mathrm{cm}^2/(\mathrm{V} \cdot \mathrm{s})$ [7]. In addition, we know $\mu_e = \frac{e\tau}{m_e}$, where m_e is the mass of the electron. So we can estimate the scattering time τ as

$$\begin{aligned}
\tau &= \frac{\mu_e m_e}{e} \\
&= \frac{(2.3 \times 10^2 \sim 7.3 \times 10^3) \times 9.11 \times 10^{-31}}{1.6 \times 10^{-19}} \frac{\mathrm{kg} \cdot \mathrm{cm}^2}{C \cdot (V \cdot s)} \\
&= \frac{(2.3 \times 10^{-2} \sim 7.3 \times 10^{-1}) \times 9.11 \times 10^{-12}}{1.6} \frac{\mathrm{kg} \cdot \mathrm{m}^2}{C \cdot (V \cdot s)} \\
&= (1.31 \times 10^{-13} \sim 4.16 \times 10^{-12})\ \mathrm{s} \\
&= (1.31 \times 10^2 \sim 4.16 \times 10^3)\ \mathrm{fs}
\end{aligned} \tag{49}$$

And the corresponding energy is $\hbar\omega = 2\pi\hbar/\tau = h/\tau = (1 \sim 31.6)$ meV.

In order to form observable Floquet states in experiments, we need the period of the pumping laser $T = 2\pi/\Omega$ to be shorter than the scattering time τ, namely $T < \tau \sim 131$ fs. Then the pumping photon energy $\hbar\Omega$ should be larger than $\hbar\omega$, namely, $\hbar\Omega > \hbar\omega \sim 31.6$ meV. This is a relatively loose restriction. In the main text, we set the photon energy $\hbar\Omega = 100$ meV to carry out Floquet calculations, which are reasonable for the formation of the Floquet states in experiments.

Supplementary Note 7. MORE DISCUSSION ON PROPOSED EXPERIMENTS

In this section, we give more discussion on our proposed experiments in the main text.

Firstly, time- and angle-resolved photoemission spectroscopy (TrARPES) remains a powerful and direct experimental technique to observe both surface and bulk Floquet band structures. As outlined in Supplementary Table 1, TrARPES has successfully detected the Floquet metallic surface state (*e.g.*, the Dirac surface state of Bi_2Se_3 and Bi_2Te_3) and the Floquet metallic bulk state (*e.g.*, the Dirac bulk state of graphene). All experiments in Supplementary Table 1 employ the (Mid-)infrared (IR) pumping to induce Floquet states (similar to our proposal, 0.1 eV for the pumping laser) and then utilize a suitable probe laser to capture the Floquet bulk or surface states. Therefore, from an experimental technology standpoint, we believe that TrARPES is possible to probe the light-induced Fermi arcs.

Technology	Reference	Pump laser	Probe laser	Material
TrARPES	[8]	0.12 eV	ultraviolet (UV) pulse	the **Dirac surface** state of Bi_2Se_3
	[9]	0.16 eV	6.3 eV	
	[10]	0.1 eV	UV pulse	the **Dirac surface** state of Bi_2Te_3
	[11]	0.65 eV	26.5 eV	the **Dirac bulk** state of graphene
	[12]	0.246 eV	26.4 eV	
	[13]	0.28 eV	21.7 eV	the **bulk** state of WSe_2
	[14]	0.34-0.44 eV	6.2 eV	the **bulk** state of black phosphorus (BP)
	[15]	0.16 eV	6.2 eV	

Supplementary Table 1. TrARPES experiments for the direct observation of Floquet states.

Secondly, we have listed some related experiments in Supplementary Table 2 to show the feasibility of detecting Kerr and Faraday rotations on the ultrafast timescales. The initial three experiments in Supplementary Table 2 all focus on non-magnetic or paramagnetic materials, where CPL is applied to break time-reversal symmetry (TRS), leading to the CPL-induced anomalous Hall effect. These studies employ Mid-IR pumping-terahertz (THz) Faraday probe spectroscopy to measure the Faraday rotation angle and deduce the CPL-induced anomalous Hall conductivity (AHC) in the frequency domain.

Moreover, we should point out that birefringence is a potential phenomenon in the Kerr and Faraday rotation measurements. However, birefringence typically exhibits anisotropy compared to Kerr and Faraday rotations. That is, in principle by rotating the half-wave plate while keeping the beam at the same spot, we can distinguish birefringence from Kerr (Faraday) signals. This allows us to extract the contribution of birefringence, which is a viable experimental treatment method [16].

Finally, We attempt to provide a brief derivation to consider the electron occupation for the AHC. Before the laser pumping, due to the presence of the TRS, the AHC $\sigma = \sum_n \int_{BZ} [f(\epsilon_n(\mathbf{k}))\Omega_n(\mathbf{k})] d\mathbf{k} = 0$, where $f(\epsilon_n(\mathbf{k}))$ is the electron occupation at the n-th band. In equilibrium, $f(\epsilon_n(\mathbf{k}))$ follows the Fermi-Dirac distribution, and $\epsilon_n(\mathbf{k})$ is the n-th band energy. Under CPL pumping, we suppose the light-induced AHC to be $\sigma' = \sum_n \int_{BZ} [f'(\epsilon_n(\mathbf{k}))\Omega'_n(\mathbf{k})] d\mathbf{k}$, and the change of AHC can be described

Technology	Reference	Material	Pump laser	Probe laser
THz Faraday probe spectroscopy	[17]	the **Dirac fermion** in Cd_3As_2	0.138 eV $\sim 10^7$ V/m	∼THz
	[18]	the massive **Dirac fermion** in $Co_3Sn_2S_2$ above the Curie temperature	0.31 eV $\sim 1.1 \times 10^8$ V/m	∼THz
	[19]	the **Dirac fermion** in bismuth	0.31 eV $\sim 2.3 \times 10^7$V/m	∼THz
	Our proposal	the **topological fermion** in CoSi	0.1 eV 4.4×10^7 V/m	∼THz

Supplementary Table 2. THz Faraday experiments related to the Floquet physics.

as:

$$\begin{aligned}
\delta\sigma &= \sigma' - \sigma \\
&= \sum_n \int_{BZ} \left[f'(\epsilon_n(\mathbf{k}))\Omega'_n(\mathbf{k}) - f(\epsilon_n(\mathbf{k}))\Omega_{\mathrm{n}}(\mathbf{k})\right] d\mathbf{k} \\
&= \sum_n \int_{BZ} \left[f'(\epsilon_n(\mathbf{k}))\Omega'_n(\mathbf{k}) - f(\epsilon_n(\mathbf{k}))\Omega'_n(\mathbf{k}) + f(\epsilon_n(\mathbf{k}))\Omega'_n(\mathbf{k}) - f(\epsilon_n(\mathbf{k}))\Omega_{\mathrm{n}}(\mathbf{k})\right] d\mathbf{k} \\
&= \sum_n \int_{BZ} \left[f'(\epsilon_n(\mathbf{k})) - f(\epsilon_n(\mathbf{k}))\right] \Omega'_n(\mathbf{k}) d\mathbf{k} + \sum_n \int_{BZ} f(\epsilon_n(\mathbf{k})) \left[\Omega'_n(\mathbf{k}) - \Omega_{\mathrm{n}}(\mathbf{k})\right] d\mathbf{k} \\
&= \sum_n \int_{BZ} \left[f'(\epsilon_n(\mathbf{k})) - f(\epsilon_n(\mathbf{k}))\right] \Omega'_n(\mathbf{k}) d\mathbf{k} + \sum_n \int_{BZ} f(\epsilon_n(\mathbf{k}))\Omega'_n(\mathbf{k}) d\mathbf{k}
\end{aligned} \tag{50}$$

As we can see from Supplementary Equation 50, the first term corresponds to the contribution from the change of the electron occupation and the light-induced Berry curvature, while the second term only arises from the light-induced Berry curvature (due to the equilibrium Fermi-Dirac distribution $f(\epsilon_n(\mathbf{k}))$, the dominate term is the momentum shift), corresponding to $\sum_{k\in\{\Gamma,R\}} \chi_k(\eta) \cdot \delta_k$ shown in the main text. Then, we analyze the contribution of the first term in Supplementary Equation 50 under different cases.

Herein, we propose to use the THz Faraday probe spectroscopy to detect the change of AHC [18, 19], the pulse duration of THz laser is on the order of magnitude of ps. In such time scale, the electronic states with higher energy away from the Fermi level will contribute little. For the light-induced sidebands around the Fermi level within the energy window $[-0.1\ \mathrm{eV}, 0.1\ \mathrm{eV}]$, the change of the electron distribution $[f'(\epsilon_n(\mathbf{k})) - f(\epsilon_n(\mathbf{k}))]$ combined with the light-induced Berry curvature (see the first term in Supplementary Equation 50) should contribute to the AHC to some extent.

In practical terms, for the massive Dirac semimetal $Co_3Sn_2S_2$ above the Curie temperature, the contribution of light-induced AHC has been confirmed from the Floquet Berry curvatures predominantly [18]. In the similar setup and system, we anticipate that the momentum shifts from the Floquet Berry curvatures in CoSi could primarily contribute to the AHC.

However, the above discussion is just a preliminary argument. The time-dependent density functional theory (TDDFT) or quantum Liouville equation with relaxation should be utilized to com-

prehensively examine the electron occupation of Floquet bands in the future.

[1] T. Zhang, Z. Song, A. Alexandradinata, H. Weng, C. Fang, L. Lu, and Z. Fang, Double-Weyl phonons in transition-metal monosilicides, Phys. Rev. Lett. **120**, 016401 (2018).

[2] B. Xu, Z. Fang, M.-Á. Sánchez-Martínez, J. W. Venderbos, Z. Ni, T. Qiu, K. Manna, K. Wang, J. Paglione, C. Bernhard, *et al.*, Optical signatures of multifold fermions in the chiral topological semimetal CoSi, Proc. Natl. Acad. Sci. U.S.A. **117**, 27104 (2020).

[3] T. Mikami, S. Kitamura, K. Yasuda, N. Tsuji, T. Oka, and H. Aoki, Brillouin-Wigner theory for high-frequency expansion in periodically driven systems: Application to Floquet topological insulators, Phys. Rev. B **93**, 144307 (2016).

[4] D. Dutta, B. Ghosh, B. Singh, H. Lin, A. Politano, A. Bansil, and A. Agarwal, Collective plasmonic modes in the chiral multifold fermionic material CoSi, Phys. Rev. B **105**, 165104 (2022).

[5] A. Zee, *Group theory in a nutshell for physicists*, Vol. 17 (Princeton University Press, 2016).

[6] B. Bradlyn, J. Cano, Z. Wang, M. Vergniory, C. Felser, R. J. Cava, and B. A. Bernevig, Beyond Dirac and Weyl fermions: Unconventional quasiparticles in conventional crystals, Science **353**, aaf5037 (2016).

[7] X. Xu, X. Wang, T. A. Cochran, D. S. Sanchez, G. Chang, I. Belopolski, G. Wang, Y. Liu, H.-J. Tien, X. Gui, *et al.*, Crystal growth and quantum oscillations in the topological chiral semimetal CoSi, Phys. Rev. B **100**, 045104 (2019).

[8] Y. Wang, H. Steinberg, P. Jarillo-Herrero, and N. Gedik, Observation of Floquet-Bloch states on the surface of a topological insulator, Science **342**, 453 (2013).

[9] F. Mahmood, C.-K. Chan, Z. Alpichshev, D. Gardner, Y. Lee, P. A. Lee, and N. Gedik, Selective scattering between Floquet–Bloch and Volkov states in a topological insulator, Nat. Phys. **12**, 306 (2016).

[10] S. Ito, M. Schüler, M. Meierhofer, S. Schlauderer, J. Freudenstein, J. Reimann, D. Afanasiev, K. Kokh, O. Tereshchenko, J. Güdde, *et al.*, Build-up and dephasing of Floquet–Bloch bands on subcycle timescales, Nature **616**, 696 (2023).

[11] M. Merboldt, M. Schüler, D. Schmitt, J. P. Bange, W. Bennecke, K. Gadge, K. Pierz, H. W. Schumacher, D. Momeni, D. Steil, *et al.*, Observation of Floquet states in graphene, arxiv preprint 10.48550/arXiv.2404.12791 (2024).

[12] D. Choi, M. Mogi, U. De Giovannini, D. Azoury, B. Lv, Y. Su, H. Hübener, A. Rubio, and N. Gedik, Direct observation of Floquet-Bloch states in monolayer graphene, arxiv preprint 10.48550/arXiv.2404.14392 (2024).

[13] S. Aeschlimann, S. A. Sato, R. Krause, M. Chavez-Cervantes, U. De Giovannini, H. Hübener, S. Forti, C. Coletti, K. Hanff, K. Rossnagel, A. Rubio, and I. Gierz, Survival of Floquet-Bloch states in the presence of scattering, Nano Lett. **21**, 5028 (2021).

[14] S. Zhou, C. Bao, B. Fan, H. Zhou, Q. Gao, H. Zhong, T. Lin, H. Liu, P. Yu, P. Tang, *et al.*, Pseudospin-selective Floquet band engineering in black phosphorus, Nature **614**, 75 (2023).

[15] S. Zhou, C. Bao, B. Fan, F. Wang, H. Zhong, H. Zhang, P. Tang, W. Duan, and S. Zhou, Floquet engineering of black phosphorus upon below-gap pumping, Phys. Rev. Lett. **131**, 116401 (2023).

[16] Y. Xu, Z. Ni, Y. Liu, B. R. Ortiz, Q. Deng, S. D. Wilson, B. Yan, L. Balents, and L. Wu, Three-state nematicity and magneto-optical Kerr effect in the charge density waves in kagome superconductors, Nat. Phys. **18**, 1470 (2022).

[17] Y. Murotani, N. Kanda, T. Fujimoto, T. Matsuda, M. Goyal, J. Yoshinobu, Y. Kobayashi, T. Oka, S. Stemmer, and R. Matsunaga, Disentangling the competing mechanisms of light-induced anomalous Hall conductivity in three-dimensional Dirac semimetal, Phys. Rev. Lett. **131**, 096901 (2023).

[18] N. Yoshikawa, Y. Hirai, K. Ogawa, S. Okumura, K. Fujiwara, J. Ikeda, T. Koretsune, R. Arita, A. Mitra, A. Tsukazaki, *et al.*, Light-induced chiral gauge field in a massive 3D Dirac electron system, arXiv preprint 10.48550/arXiv.2209.11932 (2022).

[19] Y. Hirai, N. Yoshikawa, M. Kawaguchi, M. Hayashi, S. Okumura, T. Oka, and R. Shimano, Anomalous Hall effect of light-driven three-dimensional Dirac electrons in bismuth, arXiv preprint 10.48550/arXiv.2301.06072 (2023).